Atmospheric Environment 383 (2026) 122290

Contents lists available at ScienceDirect

Atmospheric Environment

journal homepage: www.elsevier.com/locate/atmosenv

Review article

# A review of atmospheric black carbon research progress in China

Qi Zhou [a], Shunyao Wang [b], Shujun Bie [c], Junjie Cai [c], Yingjun Chen [c], Yuan Cheng [d], Xiang Ding [e], Jianwei Gu [f], Jie Li [g], Weijun Li [h], Dantong Liu [h], Jiaying Liu [a], Yue Liu [i], Jing Shang [a], Xiao Tang [g], Rui Tang [a], Yingze Tian [j], Jiandong Wang [k], Shuxiao Wang [l], Jing Wei [a], Yi Wei [a], Yaxin Xiang [a], Caiqing Yan [m], Fenfen Zhang [l], Zhouyang Zhang [k], Gan Zhang [e], Qiang Zhang [n], Yan Zhang [c], Guangcai Zhong [e], Mei Zheng [a,*]

[a] State Key Laboratory of Regional Environment and Sustainability, College of Environmental Sciences and Engineering, and Center for Environment and Health, Peking University, Beijing, 100871, China
[b] School of Environmental and Chemical Engineering, Shanghai University, Shanghai, 200444, China
[c] Department of Environmental Science and Engineering, Fudan University, Shanghai, 200433, China
[d] State Key Laboratory of Urban-rural Water Resource and Environment, School of Environment, Harbin Institute of Technology, Harbin, 150090, China
[e] State Key Laboratory of Advanced Environmental Technology, Guangzhou Institute of Geochemistry, Chinese Academy of Sciences, Guangzhou, 510640, China
[f] School of Environmental Science and Engineering, Guangdong University of Technology, Guangzhou, 510006, China
[g] State Key Laboratory of Atmospheric Environment and Extreme Meteorology, Institute of Atmospheric Physics, Chinese Academy of Sciences, Beijing, 100029, China
[h] Department of Atmospheric Sciences, School of Earth Sciences, Zhejiang University, Hangzhou, 310058, China
[i] Center for Environmental Metrology, National Institute of Metrology China, Beijing, 100029, China
[j] Key Laboratory of Urban Air Particulate Pollution Prevention and Control of Ministry of Ecology and Environment, College of Environmental Science and Engineering, Nankai University, Tianjin, 300350, China
[k] State Key Laboratory of Climate System Prediction and Risk Management, Nanjing University of Information Science and Technology, Nanjing, 210044, China
[l] State Key Laboratory of Regional Environment and Sustainability, School of Environment, Tsinghua University, Beijing, 100084, China
[m] Environment Research Institute, Shandong University, Qingdao, 266237, China
[n] Ministry of Education Key Laboratory for Earth System Modeling, Department of Earth System Science, Tsinghua University, Beijing, 100084, China

## HIGHLIGHTS

- Recent BC studies in China were reviewed, including sources, aging, mixing state, and health effects.
- Gridded BC datasets have been established, showing significant decreases of BC concentration in China during the past decade.
- Aging and different mixing states of BC strongly impact its morphology, light absorption, and health effects.
- BC exposure is associated with respiratory, cardiovascular, and neurological effects, with its toxicity varying by source types and atmospheric aging processes.

## ARTICLE INFO

*Keywords:*
Black carbon
Sources
Aging
Mixing state
Health effects
China

## ABSTRACT

Black carbon (BC) is an atmospheric pollutant that adversely affects air quality, global climate, and human health. As an important BC source region, China has achieved substantial emission reductions over the past decade through stringent clean air policies, offering a unique opportunity to study changes of BC sources and properties under rapid emission changes. Concurrently, BC research in China has progressed rapidly, shifting from studying emission sources toward atmospheric processes and health impacts. This review focuses on five key topics in BC research, including ambient concentrations, emission sources, atmospheric aging, mixing state, and health effects. Ground observation networks and gridded datasets have shown a significant decrease in BC concentrations due to clean air policies, particularly in Northern and Eastern China. Emission inventories and source apportionment studies consistently identified fossil fuel combustion as the dominant BC source in China. Laboratory, field, and modeling studies have advanced understanding of BC aging and mixing state. The health evidence from China has linked BC exposure to respiratory, cardiovascular, and neurological diseases. The rapid expansion and heterogeneity of datasets underscore the urgent need for measurement standardization and cross-regional dataset comparison. In addition, this review calls for stronger integration of measurement and modeling

* Corresponding author.
*E-mail address:* mzheng@pku.edu.cn (M. Zheng).

https://doi.org/10.1016/j.atmosenv.2026.122290
Received 18 July 2026; Accepted 9 August 2026
Available online 10 August 2026

to better study BC sources, aging, and mixing states, and highlights the need for assessing source-specific health impacts and understanding how atmospheric aging modifies BC toxicity.

## 1. Introduction

Black carbon (BC) plays a crucial role in global climate change (Adachi et al., 2010; Gustafsson et al., 2026; Huang et al., 2024; Jacobson, 2001) and regional air quality (Ding et al., 2016, 2019a; Huang et al., 2018). BC affects the climate primarily through the absorption of solar radiation and by acting as cloud condensation nuclei (CCN) that modify cloud formation and distribution (Andreae and Gelencser, 2006; Jacobson, 2004; Liu et al., 2015; Oshima et al., 2009; Zaveri et al., 2010). These effects involve complex processes, including aerosol-cloud interactions and boundary layer feedbacks (Ding et al., 2016; Winiger et al., 2016; Xu et al., 2016). Moreover, the strong light absorption by BC significantly reduces atmospheric visibility (Li et al., 2022b). It also modifies planetary boundary layer (PBL) meteorology and exacerbates haze pollution, forming a positive feedback mechanism termed the "dome effect" (Ding et al., 2016).

BC has also gained increasing recognition for its health implications. BC particles are sufficiently small to penetrate deep into the human respiratory tract. Their large specific surface area also allows efficient adsorption of toxic compounds such as polycyclic aromatic hydrocarbons (PAHs), thereby increasing human exposure to hazardous pollutants (Ali et al., 2021; Lippmann and Chen, 2009; Niranjan and Thakur, 2017). Epidemiological studies have consistently suggested that combustion-related particles, represented by BC, are closely associated with adverse health outcomes, and the evidence linking BC exposure to health risks is considered among the most robust (Janssen et al., 2011; Smith et al., 2009; Zhu et al., 2023). Given these important environmental, climatic, and health implications, BC has become a major focus of international research, resulting in a rapid increase in the number of related studies in recent years.

In China, BC has attracted growing attention due to its large emissions and significant environmental and health implications (Liu et al., 2025a; Peng et al., 2016). As one of the major BC emitters, China released an estimated 916 Gg of anthropogenic BC in 2023 based on the emission inventory from Multi-resolution Emission Inventory Model for Climate and Air Pollution Research (MEIC) (http://meicmodel.org.cn/). In response to severe haze episodes a decade ago, the Chinese government strengthened air quality management and established national standards for fine particulate matter ($PM_{2.5}$) in 2012 (Ministry of Ecology and Environment of the People's Republic of China, 2012). As an important component of $PM_{2.5}$, BC has become an important focus of scientific research and air quality management strategies. Intensive emissions have led to high BC concentrations in many regions of China, and diverse combustion sources, including residential burning, industrial activities, and traffic emissions, contribute to the complex source structure of BC (Shan et al., 2025). Furthermore, the high BC concentrations in China have also contributed to substantial public health burdens. For instance, a study estimated that the national annual BC-associated premature mortality ranged from 733,910 cases $yr^{-1}$ to 937,980 cases $yr^{-1}$ during 2000-2020 in China (Zhao et al., 2024a).

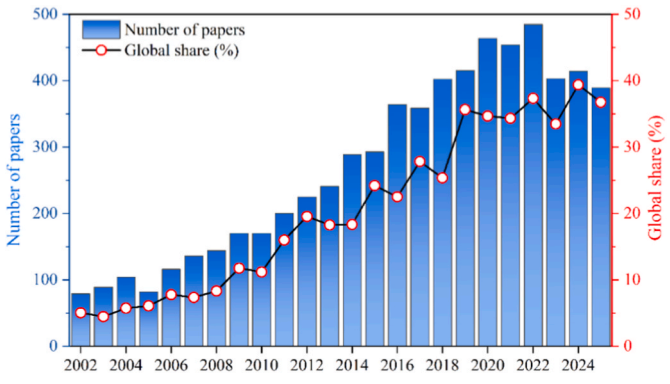


**Fig. 1.** Number of publications under the topic of atmospheric black carbon and elemental carbon contributed by Chinese authors from 2002 to 2025. Data were obtained from the Web of Science Core Collection database using the search-terms as "atmospheric" and ("black carbon" or "elemental carbon") and filtering for publication address in China.

Given these prominent features and impacts, China has become an increasingly important region for BC research and accounts for 40% of the global publications in this field by 2024 (Fig. 1). The thematic focus of atmospheric BC studies contributed by Chinese researchers has evolved substantially over time (Fig. 2). Source apportionment has consistently remained a central topic, reflecting its fundamental importance for emission control strategies, while emerging research directions such as health effects and mixing state have gained increasing attention in recent years. These trends indicate a transition from traditional emphasis on emissions and regional pollution characteristics toward a more integrated understanding of the physicochemical properties and environmental impacts of BC.

Fig. 2 shows the temporal evolution of research topics in BC-relevant studies contributed by Chinese authors. These evolving research trends, together with the growing Chinese contributions, motivate this review to synthesize current knowledge. This review focuses on five key topics of BC research, including ambient concentration, emission sources, atmospheric aging, mixing state, and health effects, in order to enhance our understanding of BC properties in ambient air and its environmental impacts. Table 1 shows a list of abbreviations for major models, datasets, and instruments.

## 2. BC concentration and spatiotemporal variability in China

Accurate quantification of BC mass concentration is fundamental for evaluating its environmental impacts. In China, ground-based observation networks have been established across different regions, enabling detailed assessments of the temporal and spatial variability of BC concentrations. Additionally, gridded BC concentration datasets have been developed in recent years by integrating multiple data sources, including ground observations, satellite retrievals, and chemical transport models. These datasets provide spatially and temporally continuous BC concentration fields, offering new opportunities to better characterize the spatiotemporal variability of BC across China.

This section reviews recent advances in both ground-based observations and gridded datasets, and examines BC concentration levels and their variability in China based on the major datasets. Furthermore, given the increasing attention in recent years to the differentiation of BC into subgroups, specifically Soot and Char, we summarize the latest developments in studies of these subgroups, especially their physicochemical properties.

### 2.1. BC concentration based on monitoring networks in China

#### 2.1.1. Definitions and measurement techniques of BC

Although various definitions of BC have been proposed over the years (Bond et al., 2013; Goldberg, 1985; Novakov, 1984; Petzold et al., 2013), a commonly used definition in current atmospheric research describes BC as a class of carbonaceous particulate matter characterized by strong light absorption, high-temperature refractoriness, thermal stability, and chain-like aggregate morphology (Bond et al., 2013; Tang et al., 2024b). Because BC is not a single chemically defined substance,

different measurement principles have led to several operationally defined BC metrics (Petzold et al., 2013). Among them, equivalent BC (eBC) is derived from filter-based and in-situ optical absorption measurements and converted to a mass concentration using an assumed mass absorption cross-section (MAC), whereas refractory BC (rBC) is measured by laser-induced incandescence and represents the refractory carbonaceous cores that incandesce under intense laser heating (Sedlacek et al., 2012).

Intercomparisons of BC measurements in China show that different analytical techniques could yield different concentrations. Larger discrepancies have been reported between eBC measured by Aethalometer and rBC measured by Single Particle Soot Photometer (SP2), with eBC/rBC ratios ranging from 1.28 in urban Xi'an to 2.49 at the remote Qinghai Lake site (Wang et al., 2014b). Differences are also observed for eBC from different optical instruments, with Aethalometer AE33-derived eBC being approximately 1.69 times higher than Photoacoustic Extinctiometer-derived eBC in Beijing (Sun et al., 2021). Therefore, BC concentrations measured using different methods should be interpreted carefully, as differently operationally defined BC metrics are method-dependent quantities.

In some studies, elemental carbon (EC) is suggested to be used as a proxy for BC due to compositional similarities (Bond et al., 2013; Liu et al., 2022b; Petzold et al., 2013; Zhang et al., 2023b). However, it should be recognized that BC is not simply equivalent to EC, as EC is determined by the thermal-optical analysis (TOA) method, which depends on the specified temperature protocol and charring correction scheme (Huntzicker et al., 1982). Based on simultaneous measurements of BC by an AE33 and EC by the Sunset semi-continuous OC/EC analyzer, a study conducted in Beijing showed a strong correlation between eBC and EC ($r = 0.90$), but eBC was generally higher than EC, with an average difference of 1.21 $\mu g\ m^{-3}$ (Liu et al., 2022b). Therefore, a simple substitution of EC for BC could introduce uncertainties in both measurements and models.

In China, BC observations are predominantly based on optical methods that quantify light absorption or laser-induced incandescence signals. These approaches can be broadly categorized into in-situ and filter-based methods (Liu et al., 2023c). In-situ methods primarily include photoacoustic spectrometry (PAS), photothermal interferometry (PTI), and laser-induced incandescence (LII) (Liu et al., 2023c). In contrast, filter-based optical methods estimate BC from light attenuation through particle-loaded filters after sampling ambient aerosols.

Filter-based optical methods are widely used in China due to their relatively high temporal resolution, good environmental adaptability, and suitability for long-term observations and portable measurements, such as in-vehicle measurements (Guan et al., 2022; Liu et al., 2020a; Sun et al., 2020; Tian et al., 2020). Liu et al. (2023c) summarized the BC studies based on optical methods in China since 2013, and the results show that approximately 61% of BC optical studies have adopted the filter-based method. As for the in-situ methods, the LII method is the

**Table 1**
List of abbreviations for major models, datasets, and instruments.

| Name | Abbreviation |
|---|---|
| Aethalometer AE33 | AE33 |
| The High-resolution Air Quality Reanalysis Dataset over China | CAQRA-aerosol |
| Chemical Transport Model | CTM |
| China High Air Pollutants Dataset | CHAP |
| Community Earth System Model | CESM |
| Community Multiscale Air Quality Modeling System | CMAQ |
| Multi-resolution Emission Inventory Model for Climate and Air Pollution Research | MEIC |
| Positive Matrix Factorization | PMF |
| Regional Atmospheric Modeling System | RAMS |
| Soot Particle Aerosol Mass Spectrometer | SP-AMS |
| Single Particle Soot Photometer | SP2 |
| Single Particle Aerosol Mass Spectrometer | SPAMS |
| Scanning Electron Microscopy | SEM |
| Tracking Air Pollution Dataset | TAP |
| Transmission Electron Microscopy | TEM |
| Weather Research and Forecasting Model Coupled with Chemistry | WRF-Chem |
| Weather Research and Forecasting Model Coupled with CMAQ | WRF-CMAQ |

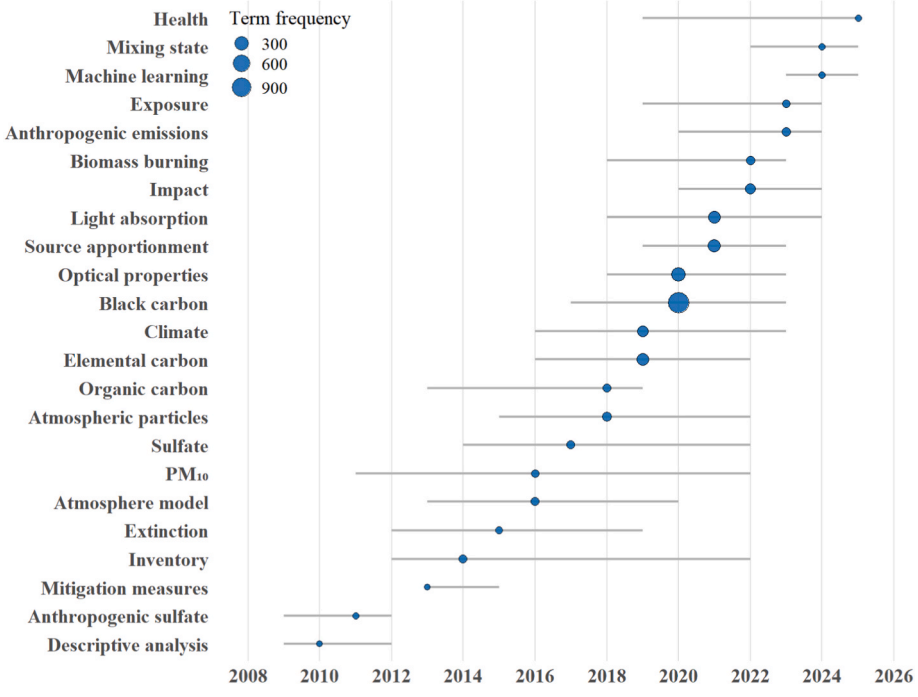


**Fig. 2.** Temporal evolution of research topics in BC-relevant studies contributed by Chinese authors from 2008 to 2025. Data are from the Web of Science Core Collection database using the search-terms as "atmospheric" and "black carbon", with author affiliations restricted to China. Bibliometric analysis was performed using the bibliometrix package (R 4.5.1). For each year, the most frequent keywords (up to two) are shown here, and geographical terms are excluded to emphasize the underlying research topics. The horizontal line denotes the interquartile range (Q1-Q3) of publication years. The circle position denotes the median year. The circle size is proportional to the term frequency.

most widely used, accounting for 33%, followed by PAS (4%) and the PTI method (2%).

However, the filter-based methods are subject to several well-recognized artifacts, including the loading effect of PM on the filter, scattering effects, and interactions between the filter membrane and the sampled particles. Regarding the measurement accuracy of BC absorption coefficient, multiple comparative studies using different instruments have been conducted in China. Zhao et al. (2020) conducted simultaneous field observations using a filter-based aethalometer (e.g., AE33) and an in-situ PAS instrument (PASS-3), and the results showed that the absorption coefficient measured by the AE33 could be three times higher than that of the PASS-3. The mixing components of BC can affect optically derived BC concentrations. For instance, secondary organic coatings can enhance BC light absorption (Chen et al., 2017a; Cui et al., 2016; Xie et al., 2019). Particle-size distribution is also an important factor contributing to uncertainty in BC concentration assessment. Even for the same BC mass concentration, different size distributions of BC can lead to different optical responses because the MAC of BC varies with particle size (Asmi et al., 2025; Zhao et al., 2022). The uncertainties of BC measurement methods further affect the accurate assessment of its radiative forcing and health effects. However, China currently lacks a unified calibration method for the BC absorption coefficient, posing challenges to the consistency and comparability of long-term observations and model simulations.

#### 2.1.2. Ground-based monitoring networks

In China, several nationwide and regional observation networks have been established to monitor aerosol components and optical properties. One of the earliest networks is the China Black Carbon Monitoring Network (CBNET), which was established in 2006 as part of the China Atmosphere Watch Network (CAWNET). CBNET has deployed dozens of stations across the country to monitor BC concentrations in different environments, including urban, rural, and background sites (Zhang et al., 2008; Zheng et al., 2025). In addition, the National Aerosol Chemical Composition Monitoring Network (NACMON) was further developed to support the "2 + 26" air pollution control strategy in the North China Plain, providing comprehensive online and offline measurements of aerosol chemical composition and optical properties in multiple cities since 2017 (Dao et al., 2019).

Based on these monitoring networks, some studies have investigated the spatiotemporal characteristics of BC concentrations across China (Guo et al., 2020; Zheng et al., 2025). Spatially, BC concentrations generally exhibit higher levels in eastern China compared to western regions, and higher in northern China than in southern regions. In addition, urban sites typically show significantly higher BC concentrations than rural and background stations, reflecting differences in energy structure, emission intensity, and population density. Temporally, BC concentrations at most sites exhibit clear seasonal patterns, with higher levels in winter and lower in summer, mainly due to enhanced combustion emissions and unfavorable meteorological dispersion conditions during cold seasons (Zheng et al., 2025).

In terms of long-term trends, BC concentrations across China have generally decreased following the implementation of the national $PM_{2.5}$ standard in 2012 and subsequent air pollution control policies, including the *Air Pollution Prevention and Control Action Plan* (2013-2017) and the *Three-year Action Plan* (2018-2020). BC concentrations in many Chinese cities, such as Beijing, Nanjing, and Guangzhou, have shown clear decreasing trends over the past decade (Liu et al., 2025b; Xie et al., 2025; Zhou et al., 2024), indicating the effectiveness of national emission mitigation strategies. Similar decreasing trends were also observed at remote background sites, such as the Waliguan Atmospheric Background Station during 2006-2015 (Dai et al., 2021), although the magnitude of reduction in total BC mass concentrations at background sites was smaller than that observed at urban and rural stations (Zheng et al., 2025).

### 2.2. BC concentration based on gridded datasets

#### 2.2.1. Three major gridded BC datasets in China

There are three major datasets available for gridded BC concentrations across China, including the High-resolution Air Quality Reanalysis Dataset over China (CAQRA-aerosol) (https://www.capdatabase.cn/), Tracking Air Pollution (TAP) (http://tapdata.org.cn/), and China High Air Pollutants (CHAP) (https://weijing-rs.github.io/product.html). These datasets differ in both spatial and temporal resolutions. CAQRA-aerosol offers a spatial resolution of 15 km and a temporal resolution of 1 h, spanning from 2013 to 2024. The TAP dataset has a spatial resolution of 10 km and a temporal resolution of 1 day, providing long-term estimates of $PM_{2.5}$ components from 2000 to the present. The CHAP dataset has the highest spatial resolution of 1 km and a temporal resolution of 1 day, covering the period from 2000 to 2020. These datasets were developed by integrating multiple sources of information, including ground observations, satellite remote sensing, emission inventories, meteorological data, and chemical transport model simulations.

Specifically, the CAQRA-aerosol dataset is developed by the Institute of Atmospheric Physics, Chinese Academy of Sciences, by assimilating observations from more than 1000 monitoring stations into chemical transport model simulations using the ensemble Kalman filter (EnKF) technique (Kong et al., 2024). The TAP dataset, developed by Tsinghua University, applies a two-step framework. First, a random forest algorithm is used to estimate gridded $PM_{2.5}$ concentrations based on multi-source data (e.g., ground measurements, satellite retrievals, meteorological data, and land-use information). Then, the CMAQ model is used to derive the concentrations of individual chemical components, including BC, by applying daily component-specific fractions of total $PM_{2.5}$ mass (Liu et al., 2022a). The CHAP dataset is primarily based on multi-source satellite remote sensing, which integrates extensive ground observations, atmospheric reanalysis data, emission inventories, and modeling to simulate air pollution across China at high resolution (Wei et al., 2023a). Validation results reported in the original dataset studies provide useful references for evaluating these datasets. The CAQRA-aerosol dataset was validated against ground observations, showing a correlation coefficient ($r$) of 0.53 for BC, a normalized mean bias (NMB) of 12.7%, and a root mean square error (RMSE) of 2.9 $\mu g\, m^{-3}$ (Kong et al., 2024). Similarly, the TAP dataset has been evaluated against ground measurements, showing $r$ as 0.59, NMB as −21.3%, and RMSE as 2.6 $\mu g\, m^{-3}$ (Liu et al., 2022a).

These gridded datasets provide a valuable basis for investigating the spatiotemporal variations and environmental impacts of BC across China. By offering continuous spatial coverage and long-term temporal records, these datasets enable researchers to quantify population exposure to BC and to examine regional differences in BC concentrations across the country. For instance, several recent studies have applied these datasets to estimate the health effects of both short-term and long-term exposure to BC in China (Jiang et al., 2024; Liu et al., 2025a; Wu et al., 2024).

#### 2.2.2. Decreasing trends in BC concentrations from three gridded datasets

Based on these datasets, the long-term trends of BC concentrations are examined across different regions. Fig. 3 illustrates the annual average BC concentrations derived from the CAQRA-aerosol, TAP, and CHAP datasets in four representative regions of China, including the North China Plain (NCP), the Yangtze River Delta (YRD), the Pearl River Delta (PRD), and the Qinghai-Tibet Plateau (QTP). All three datasets cover the same period (2013-2020) and the trends are estimated from annual average concentrations using linear regression.

From a temporal perspective, all three datasets show significant decreases in BC concentrations in the NCP, YRD, and PRD regions, reflecting the effects of recent Chinese policies aimed at reducing anthropogenic pollution in these densely populated regions. In contrast, for the QTP, only the TAP dataset presents a clear downward trend in BC

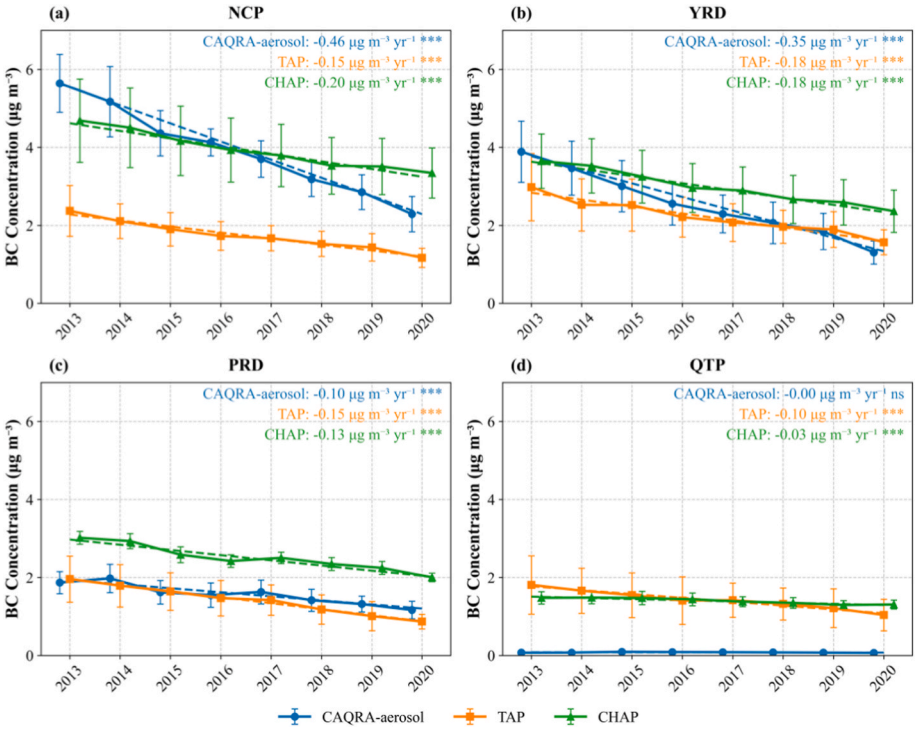


**Fig. 3.** The annual average BC concentrations derived from CAQRA-aerosol, TAP, and CHAP in four representative regions of China, including the North China Plain (NCP) region, the Yangtze River Delta (YRD), the Pearl River Delta (PRD) and the Qinghai-Tibet Plateau (QTP), from 2013 to 2020. Error bars represent the variability (standard deviation) of BC concentrations. Dashed lines represent linear trends for each dataset, with corresponding slopes (μg $m^{-3}$ $yr^{-1}$) indicating the annual rate of change for the period of 2013-2020 across the three datasets. Statistical significance of the trend is denoted by asterisks: *** indicates $p < 0.001$; "ns" indicates not significant ($p > 0.05$). The specific spatial coverage of these regions is shown in Fig. 4a.

concentrations. The CHAP dataset shows a weak decline, while the CAQRA-aerosol dataset does not show a significant decrease. The difference among these datasets in the QTP region is likely related to the scarcity of in-situ observations in this high-elevation region.

In terms of multi-year average BC concentrations during 2013-2020, the TAP dataset shows lower BC concentrations in the NCP region compared to the other two datasets, with a difference of approximately 2 μg $m^{-3}$. In the YRD region, the three datasets display different concentrations, with CHAP showing the highest levels ($2.99 \pm 0.46$ μg $m^{-3}$), followed by CAQRA-aerosol ($2.55 \pm 0.86$ μg $m^{-3}$), while TAP exhibits the lowest levels ($2.22 \pm 0.44$ μg $m^{-3}$). In the PRD region, the CHAP dataset also presents notably higher BC concentrations ($2.51 \pm 0.34$ μg $m^{-3}$) than the other two datasets, with a difference of about 1 μg $m^{-3}$, while TAP still exhibits the lowest levels ($1.42 \pm 0.38$ μg $m^{-3}$). Similarly, independent evaluations reported that TAP underestimated annual average BC concentrations by 42% in Dongguan (Li et al., 2025b) and by 20% on average across China (Zhang et al., 2025a). In the QTP region, CAQRA-aerosol shows substantially lower BC concentrations than those of the other two datasets, with a difference exceeding 1 μg $m^{-3}$.

### 2.3. BC subgroups: Char and Soot

Recent studies have provided deeper insights into the formation processes of BC, identifying two primary subgroups, Char and Soot (Cai et al., 2026a, 2026b; Han et al., 2022, 2025). Soot primarily originates from the nucleation and surface growth of gaseous precursors, forming agglomerate structures composed of aggregated nanoscale spherical monomers, whereas Char is mainly produced by the solid-phase pyrolysis and structural carbonization of fuel particles (Han et al., 2021). In most studies, Char and Soot are operationally defined using the thermal-optical reflectance (TOR) protocol, where Char is defined as EC1 minus pyrolytic carbon (PYC) and Soot is the sum of EC2 and EC3 (Cai et al., 2026a, 2026b; Han et al., 2009, 2022, 2025; Leifeld, 2007).

Research based on large-scale field data from multiple emission sources (including residential solid fuel combustion, vehicle exhaust, and industrial combustion) indicates that the combustion temperature plays a key role in regulating the composition of BC subgroups (Cai et al., 2023). A historical emission inventory of BC subgroups in China has been established, indicating that Char has dominated BC emissions over the past six decades. The reduction of Char emissions largely depends on the control of low-temperature combustion sources (Cai et al., 2023).

Furthermore, through single-particle electron microscopy analysis and oxidation flow reactor (OFR)-based aging experiments, significant differences in morphological structure, mixing state, and oxidative evolution of BC from different emission sources were revealed. The ratio of Char to Soot subgroups and their structural characteristics are crucial factors in controlling the environmental evolution and climate effects of BC (Cai et al., 2025, 2026a, 2026b). Additionally, through high-temporal-resolution observations, combined with methanol extraction-thermoluminescence analysis and the benzene polycarboxylic acid (BPCA) molecular tracer techniques, the differences in aromatic structure and optical properties between Char and Soot during haze pollution were quantitatively compared (Xu et al., 2025). Although Soot exhibits higher aromatic condensation, Char demonstrates a higher MAC, averaging approximately 1.6 times that of Soot (Xu et al., 2025). This indicates that aromatic condensation alone cannot fully explain the differences in light absorption between BC subgroups, and that structural features such as oxygen-containing functional groups may

significantly enhance light absorption (Xu et al., 2025). Such subgroup-dependent optical properties may also influence the interpretation of optically derived BC concentrations, because optical methods convert absorption signals into BC mass using an assumed MAC. This issue warrants further investigation in future studies.

## 3. BC sources in China

China has long been recognized as one of the largest emitters of BC, accounting for approximately 20-25% of global BC emissions (Wang et al., 2021b). Typical emission sources in China include residential combustion, industrial activities, transportation, and open biomass burning. In response to growing concerns over air quality, the Chinese government has implemented a range of stringent control measures that have led to a noticeable reduction in BC emissions. For instance, BC emissions in China increased from 1.11 Tg in 1962 to a peak of 3.03 Tg in 1995, followed by a gradual decline to 1.02 Tg by 2019, reflecting the effect of strengthened air pollution control measures (Li et al., 2024a).

To identify the primary sources driving reductions in BC concentrations, studies have been carried out in China, which can be broadly classified into three categories, including emission inventory-based, observation-based, and air quality model-based techniques. An overview of understanding BC sources based on each method is presented below.

### 3.1. Identifying BC sources based on emission inventories

#### 3.1.1. Source tests of BC

Focusing on the emission characteristics of BC, multiple emission sources, including residential coal combustion (Chen et al., 2005, 2006, 2009; Zhi et al., 2008), biomass burning (Peng et al., 2023b; Sun et al., 2018; Wang et al., 2023a), industrial sources (Cui et al., 2023a), and on-road and non-road mobile sources (Zhang et al., 2020a, 2021a, 2025c) have been studied and tested in China. Measurements have included emission factors, particle size distributions, BC mass, and associated organic pollutants (e.g., PAHs and volatile organic compounds). These studies revealed the significant influence of factors such as fuel type (e.g., the proportion of volatile matter in coal, differences between bituminous and anthracite coal), stove type, fuel moisture content, and combustion conditions on the formation and emission of BC from solid fuel combustion. Additionally, it was found that BC emissions from industrial sources and diesel vehicles exhibit distinct operation and process-dependent characteristics.

In addition to the land-based emission sources, the rapid growth of maritime shipping has increasingly drawn attention to BC emissions from vessels. Onboard measurements have highlighted the critical role of emission factors in accurately assessing ship contributions. Yang et al. (2023) found that real-world ship emissions in China may be underestimated and that vessel class, operating mode, and engine conditions all materially affect emission-factor estimates. Similarly, Hou et al. (2023) further showed that the emission factors of ship-emitted carbonaceous particles vary substantially with engine type, fuel type, and operating load. These results suggest that ship emission inventories remain sensitive to the representativeness of locally measured emission factors.

#### 3.1.2. Rapid development of BC emission inventories in China

Emission inventories are crucial for understanding pollutant sources and changes in emission amounts over time, and for formulating emission control strategies. Multiple emission inventories have been developed for global and regional BC emissions, including the Regional Emission inventory in Asia (REAS, 1950-2015) by Kurokawa and Ohara (2020), the Emissions Database for Global Atmospheric Research (EDGAR, 1970-2022) by Crippa et al. (2024), the Hemispheric Transport of Air Pollution (HTAP, 2000-2020) by Guizzardi et al. (2025), and the Community Emissions Data System (CEDS, 1750-2023) by Hoesly et al. (2018, 2025). Many countries also maintain their own national emission inventories, such as the National Emission Inventory (NEI) compiled by the U.S. Environmental Protection Agency and Canada's Air Pollutant Emissions Inventory (APEI) provided by Environment and Climate Change Canada (ECCC, 2025; U.S. EPA, 2026).

The compilation of emission inventories in China started later than in developed countries. One of the key events was the development of a gridded inventory by Cao et al. (2006), which provided a detailed estimate of BC emissions for China in 2000 using county-level fuel consumption statistics and locally derived emission factors. Wang et al. (2012) subsequently reconstructed BC emissions in China from 1949 to 2050. Their results showed that BC emissions increased steadily for several decades and began to level off in the mid-1990s. A widely used national emission inventory is the MEIC, developed by Tsinghua University, which has been applied to evaluate changes in anthropogenic emissions in China since 2010 (Zheng et al., 2018). Later, Tsinghua University also developed the Air Benefits and Costs Attainment Assessment System - Emission Inventory Version 2.0 (ABaCAS-EI v2.0, 2005-2021), as reported by Li et al. (2023). Another significant emission inventory is the Global Emission Modeling System (GEMS), initially developed by Prof. Shu Tao's group at Peking University. Related studies based on this inventory framework have provided high spatial resolution ($0.1^\circ \times 0.1^\circ$) emission data for multiple species with species-specific temporal coverage, including BC (Shan et al., 2025), brown carbon (Xiong et al., 2022), and PAHs (Dai et al., 2025; Shen et al., 2013).

Fig. 4 presents temporal trends and sectoral contributions of BC emissions derived from the widely used MEIC emission inventory across eleven regions in China from 2013 to 2020, including contributions from the transportation, industry, and residential sectors. Clear spatial differences can be observed among the regions. The NCP region shows the highest BC emissions throughout the study period, followed by the Southeast and Northeast regions (Fig. 4b), reflecting the combined influence of dense population, intensive industrial activities, and high residential energy consumption in these regions. In contrast, the QTP region exhibits the lowest BC emissions due to its sparse population and limited industrial development.

From a temporal perspective, most regions exhibit a declining trend in BC emissions from 2013 to 2020, particularly in major urban clusters (e.g., NCP, YRD and PRD). The reduction is mainly driven by a substantial decrease in emissions from the residential and industry sectors. This reduction can be largely attributed to the implementation of clean energy policies such as the “coal-to-gas” and “coal-to-electricity” programs in China. In comparison, emissions from the transportation sector remain relatively stable in several regions.

#### 3.1.3. Sectoral-level emission inventories of BC

At the sectoral level, residential combustion, transport, and specific industrial activities were the major primary contributors to BC emissions in China. For residential combustion, Shen et al. (2010) provided important evidence from typical Chinese stoves, reporting BC emission factors of $1.38 \pm 0.70$ g kg$^{-1}$ for crop residues and $0.23 \pm 0.36$ g kg$^{-1}$ for coals. These values are comparable with reported emission factors in other countries, such as 1.5 g kg$^{-1}$ for log wood during the start phase (Heringa et al., 2012), 1.3 g kg$^{-1}$ for wood flaming combustion (Heringa et al., 2011), 1.4 g kg$^{-1}$ for wood combustion in a three-stone stove (Islam et al., 2021), and 0.45-0.47 g kg$^{-1}$ for coal burning (Champion et al., 2017a, 2017b). They also demonstrate the dependence of residential-combustion emissions on fuel properties and combustion conditions. However, given the large variations in BC emission factors for residential combustion worldwide due to differences in fuel properties, combustion appliances, and experimental protocols (Rönkkö et al., 2023), more localized source characterization studies for residential combustion in China are still needed (Cui et al., 2023b; Luan et al., 2022; Shen et al., 2012).

For road transport, Song et al. (2012) reported a substantial increase in BC emissions from on-road vehicles between 1990 and 2009, with

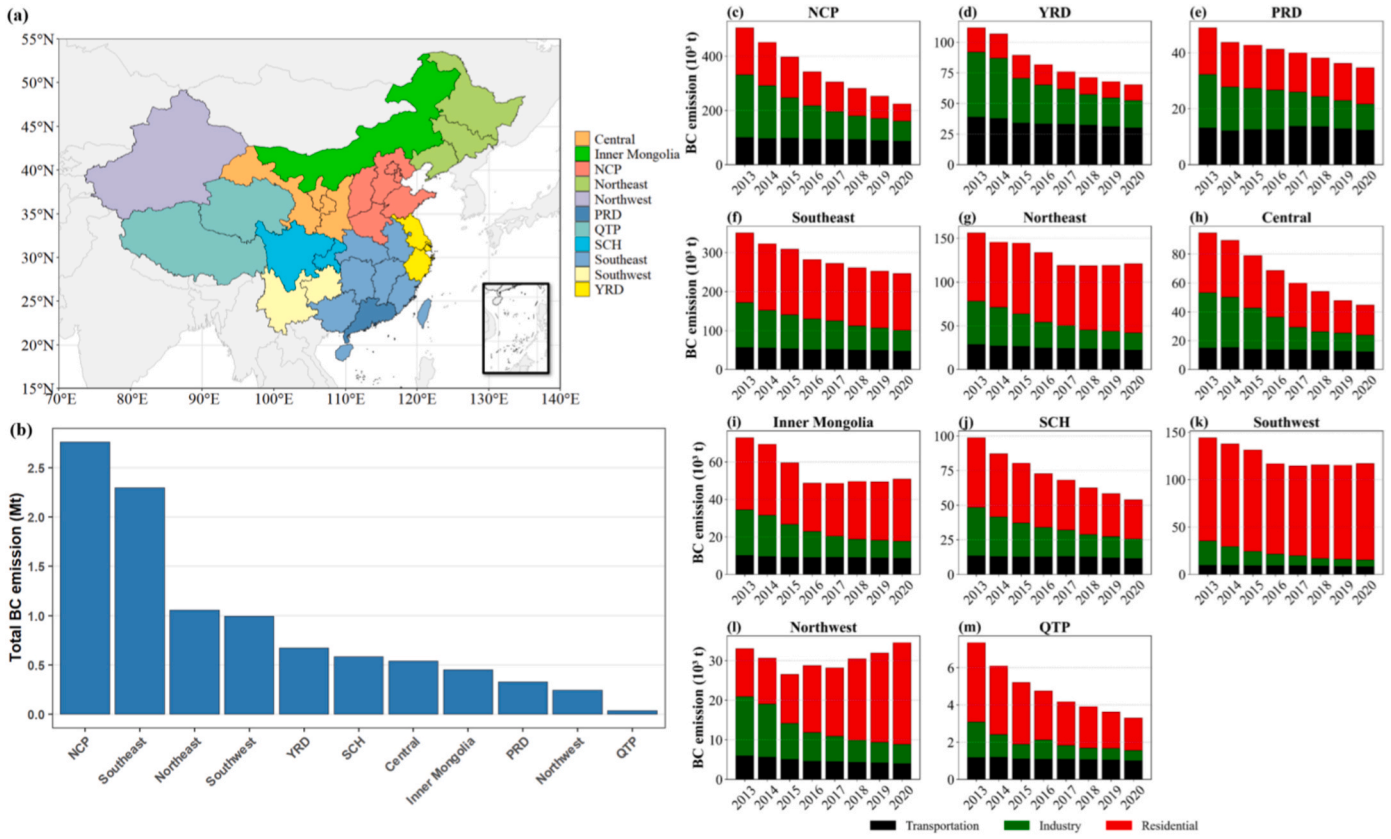


**Fig. 4.** (a) List of regions of China in this study. NCP, QTP, SCH, YRD, and PRD represent the North China Plain, the Qinghai-Tibet Plateau, the Sichuan-Chongqing region, the Yangtze River Delta, and the Pearl River Delta, respectively. (b) Total BC emissions in different regions from 2013 to 2020. (c-m) Temporal trends of BC emissions from three source sectors (transportation, industry, and residential) across eleven regions in China from 2013 to 2020.

diesel vehicles accounting for most of these emissions. This line of work was strengthened by real-world testing studies such as Zheng et al. (2015), which used portable emissions measurement systems to show how strongly traffic-related BC emission factors could depend on actual operating conditions. The industrial sector remains a significant contributor, particularly in updated national inventories where coke production and brick manufacture continue to be identified as high-emission sources (Li et al., 2024a).

As the shipping industry has expanded, growing attention has been paid to emissions from shipping activities in Chinese coastal waters. With the adoption of Automatic Identification System (AIS) data, ship emission inventories in China have evolved from local and port-specific studies to national-scale, high-spatiotemporal-resolution inventories. A national ship emission inventory for China was developed by Chen et al. (2017b) at a resolution of $0.005^\circ \times 0.005^\circ$ using a full year of AIS records for 2014. Li et al. (2018a) then traced the decadal evolution of Chinese ship emissions from 2004 to 2013, showing that BC emissions within 200 nautical miles of the coast had risen to about 29 kt $yr^{-1}$ by 2013, with large emissions concentrated around major ports and busy shipping corridors. Liu et al. (2019c) subsequently developed a 2017 ship emission inventory for East Asia at a spatial resolution of $0.1^\circ \times 0.1^\circ$, covering BC and six other species. This inventory is publicly available (https://www.capdatabase.cn). More recent inventory developments have further improved the representation of ship activity and the dependence of emission factors on operating conditions. For instance, Yi et al. (2025) developed an updated global ship emission inventory at a resolution of $0.1^\circ \times 0.1^\circ$ for the years 2013 and 2016-2021 using Shipping Emission Inventory Model (SEIM v2.2), which integrates cleaned AIS activity data, ship technical parameters, engine-load calculations, updated fuel-related emission factors, low-load adjustment, and a BC emission module to better represent ship emissions under different operating conditions. These sectoral-level inventories are essential for improving our understanding of BC emissions in China and for guiding effective mitigation strategies across sectors.

### 3.2. *Identifying BC sources based on ambient measurements*

To understand the sources of BC in the ambient atmosphere, emission inventories alone are insufficient, as BC undergoes atmospheric transport and depositional removal processes after emission. Observation-based BC source apportionment methods provide critical complementary information, with the primary approaches including the aethalometer model, carbon isotope analysis, and receptor models.

#### 3.2.1. *The aethalometer model*

The aethalometer model is a widely used approach for BC source apportionment, relying on wavelength-dependent light absorption measurements from multi-wavelength instruments. The method is grounded in the assumption that ambient BC primarily originates from two categories (e.g., biomass burning and fossil fuel combustion). Given that these sources exhibit distinct absorption Ångström exponents (α value), the model can apportion BC into biomass-derived ($BC_{bb}$) and fossil fuel derived BC ($BC_{ff}$) components based on optical absorption data (Favez et al., 2010; Sandradewi et al., 2008a, 2008b).

In early applications, this model was extensively employed in BC source apportionment studies across Europe and the United States to distinguish between $BC_{bb}$ and $BC_{ff}$ (Briggs and Long, 2016). However, coal combustion is also an important BC source in China. Therefore,

some studies have refined the aethalometer model to account for coal combustion sources. For instance, Liu et al. (2018) summarized results of source emission tests on various coal types and found that the average α value for coal combustion was 1.98, which closely resembles that of biomass burning, thus representing emissions from solid fuel combustion. Consequently, the aethalometer model was refined to further differentiate between liquid fossil fuel ($BC_{lf}$) and solid fuel ($BC_{sf}$), in addition to retaining the $BC_{bb}$ and $BC_{ff}$ classifications.

Owing to its straightforward principle and low computational cost, requiring no additional inputs such as source profiles, the aethalometer model has been extensively deployed in long-term monitoring campaigns across China. Its applications cover multiple key regions, including the Beijing-Tianjin-Hebei (BTH), YRD, central China, and PRD (Xie et al., 2025; Zheng et al., 2020; Zhou et al., 2024). For instance, a study conducted in Beijing reported a substantial reduction in both $BC_{bb}$ and $BC_{ff}$ concentrations from 2013 to 2022, with a more pronounced decrease observed for $BC_{ff}$ (Xie et al., 2025). Extending beyond single-city assessments, nationwide multi-site observations further revealed that total BC and $BC_{lf}$ (indicative of traffic-related liquid fossil fuel combustion) declined most rapidly at urban sites, whereas $BC_{sf}$ (representing solid fuel combustion, including coal and biomass burning) exhibited a sharper reduction at rural sites (Zheng et al., 2025). Such a difference indicates the spatial heterogeneity in the effectiveness of emission control policies across China.

### 3.2.2. The carbon isotope method

Radiocarbon ($^{14}C$) analysis serves as a key tool for directly apportioning atmospheric BC between its two primary sources, namely biomass burning and fossil fuel combustion. Fossil fuels (e.g., coal and oil), being millions of years old, are completely depleted in $^{14}C$ and are thus termed "$^{14}C$-dead". In contrast, biomass burning (e.g., wood and crop residues) emits carbon that was recently fixed from the atmosphere, thus preserving a "modern" $^{14}C$ signature (Currie et al., 2002; Masiello et al., 2002). By measuring the $^{14}C/^{12}C$ ratio of BC in ambient particles using accelerator mass spectrometry, the fraction of modern carbon ($f_M$) can be determined. This $f_M$ value can be used in a binary mixing model to quantitatively deconvolve the contributions from biomass burning ($f_{biomass} \propto f_M$) and fossil fuel combustion ($f_{fossil} = 1 - f_{biomass}$), providing a direct, observation-based constraint on BC sources (Gustafsson et al., 2009; Szidat et al., 2006).

For radiocarbon-based source apportionment, it is essential to quantitatively isolate BC from the complex aerosol matrix. This isolation is challenging because BC comprises a heterogeneous mixture of combustion-derived carbonaceous compounds with varying physicochemical properties (Elmquist et al., 2006; Masiello, 2004). Several methods have been developed for this purpose, including chemo-thermal oxidation (CTO) (Gustafsson et al., 2001; Zencak et al., 2007), TOA (Chen et al., 2013; Zhang et al., 2012), hydropyrolysis (Zhang et al., 2019), and the BPCA method (Yi et al., 2023, 2024).

In addition to radiocarbon, stable carbon isotopes ($\delta^{13}C$) offer complementary information on fuel types, as $\delta^{13}C$ values of BC from different sources exhibit significant variability, making it a useful tracer for source apportionment. For instance, $\delta^{13}C$ values for vehicle emissions have been reported as $-25.17 \pm 0.40$ ‰ (Chen et al., 2012). Building on this, the dual-carbon isotope approach (combining $\delta^{13}C$ with $^{14}C$) further refines source apportionment by expanding the classification from two sources (biomass burning and fossil fuel) to three categories (biomass burning, coal combustion, and liquid fossil fuel combustion). This approach has been widely applied in source apportionment studies across China (Cao et al., 2017; Geng et al., 2023).

Application of carbon isotope analysis has revealed that fossil fuel combustion accounts for a relatively high fraction of BC sources in China, while biomass burning also contributes significantly, typically in the range of 20-50% (Jiang et al., 2020). For instance, Yu et al. (2018) reported that fossil fuel combustion contributed 69-82% of BC in the BTH region across different seasons. Similarly, a recent long-term study (2008-2018) in the PRD region revealed that approximately 70% of BC originated from fossil fuel combustion (Liu et al., 2025b). Furthermore, Liu et al. (2025b) showed that clean air actions implemented in China during 2014-2018 led to a 41% reduction in the annual average BC concentration in the PRD region compared with the 2008-2013 period. This decline resulted from multi-source emission reductions, with BC from coal combustion, oil combustion, and biomass burning decreasing by 43%, 43%, and 34%, respectively.

### 3.2.3. Receptor models

Receptor models, notably chemical mass balance (CMB) and Positive Matrix Factorization (PMF), are used to apportion BC sources based on the chemical composition of particulate matter measured at receptor sites. By incorporating a diverse array of chemical source tracers (e.g., organic and elemental carbon fractions, water-soluble ions, and specific organic tracers such as levoglucosan, hopanes, and polycyclic aromatic hydrocarbons), these models can resolve contributions from major source categories, including traffic emissions, coal combustion, biomass burning, and industrial activities. Compared with CMB, which requires well-characterized local source profiles that are often difficult to obtain, PMF does not rely on a priori source profiles. As a result, PMF has become a widely applied receptor model in recent BC source apportionment studies in China (Chen et al., 2023b; Fang et al., 2016; Liu et al., 2021b, 2021c; Zhou et al., 2025).

PMF has been applied to BC source apportionment across various regions in China, consistently identifying fossil fuel combustion as the dominant contributor, with traffic emissions and coal combustion representing the largest fractions. Biomass burning also plays an important role, particularly during wintertime or in rural areas where residential heating and agricultural residue burning are prevalent (Huang et al., 2015; Zhou et al., 2025). Beyond these common source types, PMF enables the identification of region-specific sources. For instance, studies in Tianjin and Guangzhou have demonstrated that vehicular emissions dominate BC contributions, supplemented by coal combustion and port-related shipping emissions (Dai et al., 2023; Huang et al., 2022). In inland cities such as Xi'an, typical sources such as fireworks can contribute substantially to BC loadings during pollution events (Lin et al., 2022).

Furthermore, PMF has increasingly been integrated with advanced measurement techniques, including Soot Particle Aerosol Mass Spectrometer (SP-AMS) and carbon isotope analysis, enabling improved discrimination of BC sources and more detailed characterization of the mixing states and atmospheric aging processes (Liu et al., 2019a, 2023d). Such combined approaches enhance the interpretability of PMF-resolved factors and reduce uncertainties in source identification by providing complementary chemical constraints. For instance, the integration of dual-carbon isotope analysis with PMF has been employed in Beijing and its southwest upwind rural site, Gucheng, to distinguish fossil fuel from non-fossil contributions, revealing the persistent dominance of fossil sources while further separating residential coal combustion from heavy oil combustion (Yang et al., 2025a). These multi-technique frameworks mark a significant advance from simple factor attribution toward chemically and isotopically constrained source resolution.

To date, the application of receptor models for BC source apportionment in China has evolved from traditional single-method analyses toward integrated multi-tracer and multi-instrument frameworks centered on PMF. This evolution has substantially improved the robustness and source resolution of apportionment results, providing critical scientific support for the design of targeted emission control strategies. Nevertheless, significant uncertainties remain. Key challenges include factor interpretability, rotational ambiguity inherent in

PMF solutions, and the sensitivity of results to the selection and quality of input species (Yang et al., 2025a). Future studies should emphasize the systematic evaluation of these uncertainties, the harmonization of source marker datasets, and the chemical specificity of isotope and mass spectral tracers.

### 3.3. Identifying BC sources based on numerical models

Observation-based source apportionment is inherently constrained to site-specific measurements, highlighting the need for numerical models to characterize the spatial distribution of BC sources and quantify regional transport. Atmospheric models such as CMAQ, WRF-Chem, and GEOS-Chem have been used to simulate the BC emissions, transport, and deposition based on emission inventories and meteorological fields. Source contribution in previous modeling studies is commonly performed using sensitivity simulations, in which emissions from specific regions or sectors are selectively reduced or removed and compared against a baseline case (Dunker et al., 1996). While this approach provides approximate estimates of source influences, it generally requires multiple model runs and may be affected by nonlinear atmospheric chemical and physical processes. To better quantify source contributions, tagged tracer techniques have been increasingly applied in BC source-receptor studies. These techniques label emissions from specific regions or sectors as tracers and track their transport and aging processes within the model (Qi and Wang, 2019b; Wang et al., 2009, 2014a).

With continued advances in modeling methodologies, numerical models have become an essential tool for investigating BC transport processes and source contributions. Compared with in-situ measurements, numerical models provide a distinct advantage in resolving BC source contributions over large spatial scales. For instance, a study based on the CMAQ model quantified the relative importance of six major emission sectors of BC across China, and found that the residential sector was the dominant source, followed by the industrial and transportation sectors (Wang et al., 2021b). Using the GEOS-Chem model, Qi and Wang (2019a) further evaluated the contribution of fossil fuel combustion and biomass burning to global BC, suggesting a higher fraction of biomass burning BC in the Southern Hemisphere ($50 \pm 11\%$) than in the Northern Hemisphere ($35 \pm 14\%$).

Another key strength of numerical modeling lies in its ability to separate local emissions from regional transport, which is essential for understanding both the export of BC from source regions and the influence of external inputs on receptor regions. For instance, a recent study by Deng et al. (2026) reported a significant decrease in China's contribution to Arctic BC from 2009 to 2022 using the GEOS-Chem model. Their results highlighted the beneficial impact of China's BC emission reductions on Arctic warming mitigation, contributing to an estimated $0.02\ W\ m^{-2}$ decrease in the direct radiative effect during the Arctic haze season. Meanwhile, modeling studies also revealed the importance of long-range transport from outside China in shaping regional BC mass in China. Over the Tibetan Plateau, the majority of anthropogenic BC was found to originate from South Asia, contributing 40-80% of BC concentration during the non-monsoon season (Yang et al., 2018). In South China, emissions from Southeast Asia represent an important external source of BC, particularly for BC from biomass burning. Fang et al. (2020) reported that BC from Southeast Asia can account for 80% of the BC column burden in the biomass burning sector.

In addition, modeling studies have further quantified the inter-regional transport of BC within China, demonstrating that emissions from northern China can influence BC levels in eastern and even southern China. Under cold-front conditions, air masses can transport BC from the NCP to the downstream YRD, contributing more than $1\ \mu g\ m^{-3}$ to BC concentrations in YRD (Lu et al., 2023). Meanwhile, studies have shown that about 90% of BC in North China is attributed to local emissions, whereas up to 35% of wintertime BC in South China can be traced back to emissions from North China (Yang et al., 2017).

Despite these advantages, substantial uncertainties remain in model-based studies. Multi-model intercomparison studies indicate large variability in simulated BC distributions and radiative effects. At the global scale, the Atmospheric Chemistry and Climate Model Intercomparison Project (ACCMIP) showed that models generally reproduced observed BC concentrations better in mid-latitude regions such as Europe and North America, but exhibited large biases in remote and high-latitude regions, particularly in simulating Arctic BC in winter and spring (Lee et al., 2013). Similarly, the Aerosol Comparisons between Observations and Models Phase III (AeroCom Phase III) further reported large inter-model differences in aerosol absorption, with the simulated BC contribution to aerosol absorption optical depth (AAOD) ranging from 36% to 84% among models (Sand et al., 2021).

At the regional scale, the Model Inter-Comparison Study for Asia Phase III (MICS-Asia III) provided a quantitative evaluation of 14 chemical transport models over East Asia and found considerable inter-model differences in BC performance (Chen et al., 2019). Different models performed best for different evaluation metrics, with WRF-Chem v3.6.1 achieving the highest correlation with observations ($r = 0.80$), WRF-CMAQ v5.0.2 producing the smallest normalized mean bias (NMB = 1.0%), and RAMS-CMAQ v4.6 yielding the lowest RMSE ($2.64\ \mu g\ m^{-3}$). However, the multi-model ensemble still underestimated BC, with $r = 0.73$, NMB = −17.0%, and RMSE = $2.77\ \mu g\ m^{-3}$, indicating persistent systematic bias across models. Observational constraints can partially reduce these uncertainties. For instance, GEOS-Chem simulations constrained by carbon isotope measurements reproduced biomass burning contributions to BC within a factor of two in most regions, although they underestimated the biomass burning contribution in Europe by 63% (Qi and Wang, 2019a). These findings indicate the importance of performing inter-model comparison and adding more observational constraints.

## 4. Atmospheric aging of BC

Once emitted into the atmosphere, BC undergoes a series of physical and chemical aging processes during transport. Fresh BC particles, primarily from incomplete combustion of carbonaceous material (e.g., fossil fuel, biofuel, and biomass), are gradually coated with sulfate, nitrate, ammonium and organic compounds (Oshima et al., 2009; Tan et al., 2020). This coating process alters BC's mixing state from externally mixed to internally mixed (China et al., 2013; Oshima et al., 2009). Meanwhile, aging pathways encompassing evaporation, condensation, coagulation, and photochemical oxidation convert initially hydrophobic fresh BC into hydrophilic particles (He et al., 2015, 2016; Matsui et al., 2013; Oshima et al., 2009; Oshima and Koike, 2013; Riemer et al., 2010; Zhang et al., 2016).

Among BC aging processes, physical aging primarily involves gaseous pollutant adsorption, condensation and particle coagulation, whereas chemical aging mainly refers to multiphase reactions between BC and reactive species such as $SO_2$, $NO_x$, $O_3$, $H_2SO_4$, and $HNO_3$ (Bond et al., 2013; Jiang et al., 2019; Tan et al., 2020). BC particles possess a porous surface, which provides large reaction interfaces and abundant active sites to facilitate heterogeneous reactions (Monge et al., 2010). Meanwhile, the redox and catalytic properties of BC can promote reactions that are kinetically unfavorable in the gas phase. Heterogeneous aging reactions have emerged as a research focus due to their interaction with atmospheric reactive trace gases. These interfacial processes act as an efficient pathway for gaseous pollutant partitioning and removal, while simultaneously driving the formation of secondary aerosol constituents (Ma et al., 2015). Furthermore, heterogeneous reactions can modify BC surface characteristics and thus alter its physicochemical properties such as mixing state, chemical composition, and hygroscopicity. These surface modifications may ultimately reshape BC's environmental and health impacts. Accordingly, systematic exploration of the heterogeneous aging mechanisms of BC is critical for evaluating its radiative forcing, climate effects and toxicological impacts. Fig. 5 provides examples of measurement and modeling studies for BC atmospheric aging in China.

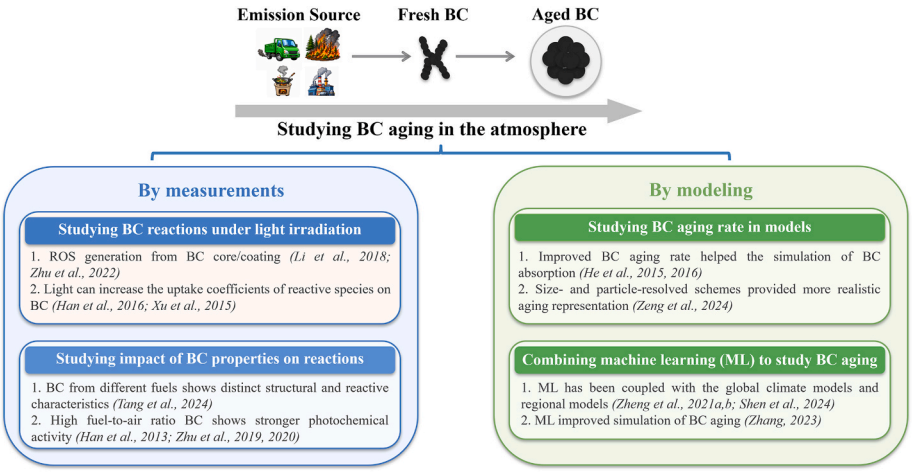


**Fig. 5.** Examples of measurement and modeling studies for BC atmospheric aging in China. Details are provided in Sections 4.1, 4.2, and 4.3.

### 4.1. Heterogeneous reactions of BC

#### 4.1.1. Dark heterogeneous reactions

The reaction kinetics of gaseous species on BC surfaces are commonly evaluated using the uptake coefficient (γ) as a core parameter. The uptake of $NO_2$ on BC surfaces has garnered extensive research attention due to the formation of reactive nitrogen species such as HONO and NO. As the predominant reaction product, HONO is generated via the redox reaction between $NO_2$ and reduced surface functional groups on BC with the participation of H atoms from water molecules (Longfellow et al., 1999). This reaction simultaneously induces the generation of nitrogen- and oxygen-containing functional groups on BC surface, yet limited attention was paid to the evolution of BC itself in these early studies.

Heterogeneous reactions between $O_3$ and BC were initially investigated to assess their influences on stratospheric ozone chemistry. In the troposphere, such reactions proceed at a lower rate compared with $NO_2$-BC reactions, thereby imposing negligible effects on urban ozone concentrations (Aklilu and Michelangeli, 2004). CO, $CO_2$ and other products can be generated during the reactions between $O_3$ and BC, indicating that BC acts as a reactant alongside the formation of various oxygen-containing functional groups (Daly and Horn, 2009; Li et al., 2013). Additionally, heterogeneous reactions of $SO_2$ on BC surfaces may contribute to atmospheric sulfate formation, and BC can act as either a catalyst or a reactant (He et al., 2018; He and He, 2020).

Heterogeneous reactions between BC and atmospheric reactive species generally follow the Langmuir-Hinshelwood mechanism (Wei et al., 2001). The initial uptake coefficient is high but decreases rapidly due to the saturation of reactive sites. The consumption or blockage of reactive sites by surface products inhibits sustained reaction progression. Therefore, except for the initial stage, these reactions exert only a minimal impact on atmospheric trace gas concentrations, and are insufficient to act as dominant sources of HONO and other reactive species (Lelièvre et al., 2004; Mak et al., 2007; Wei et al., 2001).

#### 4.1.2. Heterogeneous reactions under light irradiation

Unlike dark heterogeneous reactions on BC, which feature sluggish kinetics driven by rapid deactivation of surface active sites, light irradiation can markedly elevate BC reactivity and prolong the reaction duration. This is mainly because both the carbonaceous core (Li et al., 2018b; Zhu et al., 2022) and the outer coating (Han et al., 2012) of BC are photoactive and can generate various reactive radicals, thereby further boosting heterogeneous reactions.

Light irradiation can increase the uptake coefficients of atmospheric reactive species on BC. For instance, Zelenay et al. (2011) found that $O_3$-aged BC can be reactivated upon light irradiation, with the uptake coefficient four times higher than that under dark conditions, accompanied by an increase in surface oxygenated species (Han et al., 2016). Light irradiation can also trigger reactions between $O_2$ and BC, which are inactive in the dark, with the rate exceeding that of $O_3$ with BC under dark conditions (Han et al., 2012). In the reaction between diesel BC and $SO_2$, light enhances the S=O signal but has little effect on the initial uptake coefficient (Zhang et al., 2022c). Moreover, UV irradiation further strengthens the oxidative uptake of $SO_2$ by $O_3$-aged BC (Xu et al., 2015). Zhang et al. (2023a) proposed that surface photo-oxidation is the dominant pathway for $SO_2$ reaction on BC. Additionally, model simulations integrating BC-associated photo-heterogeneous reactions yielded modeled HONO concentrations that better matched field observational data (Zhang et al., 2021b), underscoring the critical role of light-induced BC heterogeneous reactions in modulating atmospheric reactive gas budgets.

Light irradiation also alters the reaction products. For instance, $SO_2$ reacts with BC to form ionic sulfate under dark conditions but covalent sulfate under illumination (Chughtai and Smith, 1994). Nitrogen-containing intermediates produced from the heterogeneous reaction of $NO_2$ on BC can undergo photolysis to produce HONO and NO (Guan et al., 2017; Han et al., 2013a). The OH radical generated from HONO photolysis can further promote BC aging and possibly subsequent atmospheric oxidation processes.

#### 4.1.3. The impact of BC properties on heterogeneous reactions

The surface properties of BC particles strongly affect their heterogeneous reactivity and are mainly determined by fuel type and fuel-to-air (F/A) ratio. BC emitted from diverse combustion fuels shows distinct structural and surface characteristics (Daly and Horn, 2009; Tang et al., 2024a). For instance, biofuel-derived BC is generally more amorphous and more reactive (Liati et al., 2012), while commercial BC is less reactive due to its lower heteroatom content and higher graphitization degree (Atribak et al., 2010).

For BC generated from the same fuel, the F/A ratio is a key parameter controlling its physicochemical properties and heterogeneous reactivity. In reactions with $NO_2$, BC with a high F/A ratio shows stronger photochemical activity, as reflected by enhanced $NO_2$ uptake and increased HONO and NO formation (Han et al., 2013b). Such F/A ratio-dependent effects are governed by the abundance of surface reactive sites, which is correlated with the content and oxidation degree of organic carbon (OC). Typically, BC with a high F/A ratio possesses a higher OC content (Zhu et al., 2020) and a lower OC oxidation degree (Muñoz and Rossi, 2002). This feature endows BC with abundant reduced sites and a low degree of surface oxidation, which favors heterogeneous reactions between BC and oxidative gaseous species. Hence, the F/A ratio also exhibits a linear relationship with BC reactivity toward $O_3$ (Chughtai et al.,

2002), thus making high-F/A BC more susceptible to $O_3$ aging (Zhu et al., 2019).

Surface coatings on BC also modulate heterogeneous reactions. For instance, $H_2SO_4$ coatings have little effect on $NO_2$ uptake coefficients but suppress HONO release and $HNO_3$ uptake (Loukhovitskaya et al., 2013). Moreover, $H_2SO_4$ coatings can shield BC from oxidant attack and hinder the oxidation of surface PAHs (Ray et al., 2018). Differently, glutaric acid coatings facilitate $NO_2$ uptake and subsequent HONO production, while pyrene coatings show negligible impacts (Khalizov et al., 2010). Collectively, BC particles are highly active in atmospheric heterogeneous reactions, and their surface properties play a critical role in regulating these multiphase processes.

### 4.2. Modeling studies on BC aging

#### 4.2.1. BC aging rate in the CTM model

Currently, the BC aging rate in the chemical transport model (CTM) is defined as the timescale over which BC-containing particles are fully transformed into particles that can be activated as CCN (Riemer et al., 2010). The default global models (e.g., GEOS-Chem) employed a default aging rate (e.g., 1.15 days) for BC aerosol, which may introduce substantial uncertainties in simulated BC distributions and radiative effects (Nordmann et al., 2014; Qi et al., 2017; Qi and Wang, 2019a). For regional models (e.g., WRF-CMAQ), it is assumed that aerosols are fully internally mixed and BC aging is neglected, leading to an overestimation of BC absorption enhancement by 20-250% (He et al., 2015, 2016).

A simple parameterization for the BC aging process (e.g., coating with sulfate at a linear rate) was applied in global models, which achieved good agreement with both surface and airborne measurements, thereby mitigating the overestimation of BC concentrations in earlier models (Liu et al., 2011; Zhang et al., 2015). Previous studies also described BC aging rates through microphysical processes of condensation, coagulation, photochemical oxidation, hygroscopicity, and changes in CCN activity (Liu et al., 2011). By implementing a microphysics-based BC aging parameterization into the aerosol module of the GEOS-Chem model, the aging process could be numerically simulated. Comparisons with results from airborne measurements showed that the microphysics-based aging module significantly improved simulated BC concentrations, effectively reducing the overestimation of BC absorption (He et al., 2016). Moreover, the aging rates calculated by the microphysics-based module were found to be 2 to 6 times higher than those from the default model (e.g., with an aging e-folding time of 1.2 days) (He et al., 2015, 2016). However, the simplifications might lead to uncertainties in aging rates in tropical regions and the lower troposphere (He et al., 2015, 2016). Hence, these approaches were limited by the bulk aerosol treatment in the GEOS-Chem model, which simplified atmospheric chemistry without considering size-resolved BC aerosol.

#### 4.2.2. Studying BC aging using size- and particle-resolved aerosol module

To more accurately simulate the aging process of BC aerosols, parameterization with high-resolution size- or particle-resolved dataset was recommended. The two-dimensional sectional aerosol model has been incorporated into the regional models (e.g., WRF-Chem), which introduced a BC mass fraction dimension into the traditional size-resolved modeling framework (Matsui et al., 2013). Studies have shown that representing the aging process of BC significantly reduced the overestimation of light absorption coefficients (−20%), the BC heating rate (−10%), and consequently reduced the overestimation of atmospheric radiative forcing ($-3.0\ W/m^2$) (Matsui, 2016; Matsui et al., 2013). However, the limitations of this approach lay in its inability to characterize the specific coating compositions from the BC core. Moreover, the indirect radiative effects of cloud-aerosol interactions were not considered in three-dimensional air quality models.

To address the gap, the particle-resolved Monte Carlo model for simulating aerosol interactions and chemistry (PartMC-MOSAIC) was used to rigorously simulate the evolution of BC aerosol aging and the associated optical and CCN activation properties in an idealized urban plume (Zaveri et al., 2010). Meanwhile, the aging time scales of BC were explicitly calculated using the PartMC-MOSAIC model (Riemer et al., 2010). The particle-to-particle diversity and deviations from the core-shell approximation in models were needed when assessing the radiative effects of BC (Fierce et al., 2016, 2020). Observational results also provided direct evidence that the heterogeneity of particle-to-particle mixing can reduce the light absorption enhancement of BC aerosols, with a deviation of up to approximately 24% under background conditions (Zeng et al., 2024). Hence, particle-resolved models showed significant potential for future modeling. However, calculating the evolution of individual particles in the atmosphere required substantial computational power and large data storage, resulting in extremely high costs. Currently, the key limitation of particle-resolved models is their difficulty in implementing or extending into existing three-dimensional numerical models, such as regional or global climate models.

### 4.3. Machine learning and physics constraints coupled with CTM model

Given the prohibitive computational cost of conventional CTM-based modeling for large-scale applications, previous studies have attempted to use machine learning (ML) trained with high-resolution particle-resolved simulations in global models (e.g., CESM/CAM) to represent the aging process of BC aerosols (Hughes et al., 2018; Zheng et al., 2021a).

Recently, a global model was developed for estimating BC aging by coupling machine learning with a particle-resolved model (Zheng et al., 2021b). The AI and physics-constrained module integrated with BC aging process calculations from particle-resolved to global simulations using the CESM model, yielding a global annual mean BC mixing state index of 13-94% and enabling spatiotemporal mapping of BC aging (Zheng et al., 2021b). Similarly, an ML model learned from particle-resolved simulations was coupled to the CESM model, leading to a 20% reduction in BC activation fraction and a 4% increase in BC burden (Shen et al., 2024b). However, the limitations of the above studies included the lower spatiotemporal resolution (~110 km), the absence of $NO_3^-$ and $NH_4^+$ in the CESM aerosol module, and the lack of validation against field observations.

The BC mixing state index trained from particle-resolved simulations has been implemented in the WRF-CMAQ model, indicating that an ML-based module can effectively predict BC aging process in the atmosphere (Zhang, 2023). Compared with field observations, the NMB values of simulated BC aging and light absorption enhancement factor were 13.0% and 14.8%, respectively, which proved that the ML-based module can better represent BC aging process and significantly reduce the overestimation of optical properties (Zhang, 2023). Hence, the integration of ML model and physics-constrained modules into global and regional models demonstrated great potential in simulating BC aging process in the atmosphere.

## 5. BC mixing state

Uncertainties remain in estimating the climate forcing and health effect associated with BC, primarily due to its complex mixing state. For instance, uncertainties remain in quantifying BC absorption enhancement factor ($E_{abs}$) and overall climate impact, such as BC absorption aerosol optical depth ($BC_{AAOD}$) and direct radiative effect (DRE) (Li et al., 2024b). A critical source of these uncertainties lies in the over-simplified representation of BC's complex microphysical properties (e.g., mixing structures) in current climate models.

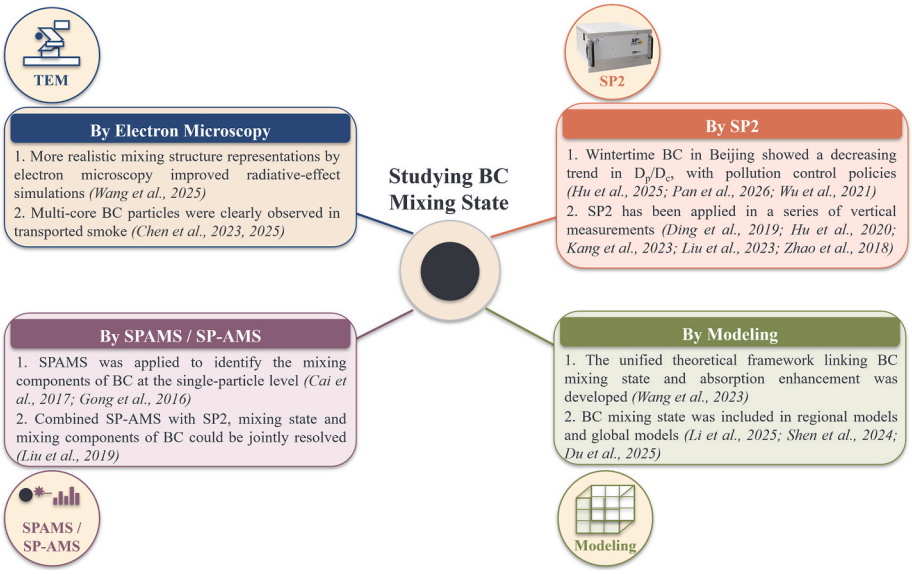


**Fig. 6.** Examples of major methods to study BC mixing state in China. Details are given in Sections 5.1 and 5.2.

Earlier studies often regarded BC mixing state as a simple distinction between external and internal mixing status. Later work adopted a more detailed description, including coating thickness, particle-to-particle heterogeneity, morphology, and atmospheric aging (Pang et al., 2022; Wang et al., 2021a, 2025). To date, many observational studies in China have provided strong evidence linking these mixing state characteristics to BC optical properties. Peng et al. (2016) showed that BC absorption and direct radiative forcing can be markedly enhanced under polluted urban conditions, largely associated with increased coating thickness during atmospheric aging. Zhang et al. (2018) further reported that the light absorption capability of BC-containing particles in Beijing increased with pollution level, which was attributed to enhanced internal mixing and thicker coatings.

The degree of BC mixing state strongly influences its physicochemical properties, hygroscopicity, and atmospheric lifetime, thereby affecting its radiative effects and environmental impacts. For instance, the coating of scattering materials can enhance BC light absorption by a few percent to more than 100%, depending on the mixing state (Chen et al., 2025; Wang et al., 2025). Understanding the mixing state of BC has therefore become an important research topic, which has been investigated through both measurements and model simulations. Fig. 6 provides examples of major methods to study BC mixing state in China.

## 5.1. Measurement of BC mixing state

In China, significant efforts have been made during field observations to gain insights into BC mixing state under real atmospheric conditions. To date, various analytical techniques have been applied in measuring the mixing state of BC particles (Fig. 6). A major challenge is to distinguish BC-containing particles from the bulk aerosol and characterize their properties at the single-particle level. Some measurement techniques have been developed, and they can be broadly categorized into three main approaches. The electron microscopy-based technique, combined with single-particle sampling, provides direct visualization of particle morphology and mixing structures, offering detailed insights into the physical configuration of BC-containing particles (Pang et al., 2022; Wang et al., 2021a, 2025). The method based on SP2, relying on laser-induced incandescence, enables quantitative determination of rBC mass at the single-particle level and is widely used to infer coating thickness and mixing state (Kang et al., 2023; Liu et al., 2019a, 2020b). Last, the Single Particle Aerosol Mass Spectrometer (SPAMS)-based method allows characterization of the chemical components associated with BC, thereby revealing the mixing of BC with organic and inorganic species (Zhou et al., 2022). Together, these approaches provide information on BC mixing state from physical and chemical perspectives.

### 5.1.1. Characterizing BC mixing state by electron microscopy

Electron microscopy (e.g., TEM/SEM) provides one of the most direct approaches for resolving the mixing state of BC at the single-particle level, offering detailed information on particle morphology (Fu et al., 2012; Li et al., 2016). Unlike bulk or indirect measurements, electron microscopy enables visualization of the physical configuration of BC-containing particles, revealing a wide range of complex mixing structures that cannot be captured by simplified assumptions. These include fractal aggregates with varying compactness, partially or fully embedded BC cores within coatings, and the presence of multiple BC cores within a single particle. Such observations provide critical constraints on how BC mixing state can influence its optical properties and radiative effects.

A key morphological parameter that can be measured by electron microscopy is the fractal dimension ($D_f$), which indicates the compactness of the aggregate (Wang et al., 2025). The degree of coating is normally quantified by the particle-to-core diameter ratio and the embedded fraction (F) (Wang et al., 2025). F ranges from 0 to 1, with 0 representing BC particles barely covered by any coating, and 1 representing BC particles that are entirely covered by coating (Wang et al., 2021a). Compared with the traditional core-shell assumption in the global climate model, one recent study indicates that more realistic multi-mixing structure representation can enhance the direct radiative effect by 24.9% to 199.8% at the single particle level by using the observed $D_f$ and F (Wang et al., 2025).

Electron microscopy provides direct evidence for multiple BC cores within a single particle, a previously overlooked mixing structure. Observations of long-range transported wildfire smoke plumes revealed that a significant fraction (e.g., 21%) of BC-containing particles contain multiple BC cores ($n_{core} > 1$) (Chen et al., 2025). This multi-core structure becomes dominant for particles with total diameters greater than 400 nm and cumulative BC core diameters greater than 200 nm (Chen et al., 2023c). This structure fundamentally differs from the single-core assumption and has profound implications for light absorption.

#### 5.1.2. Characterizing BC mixing state by SP2

The SP2 instrument enables the online and continuous measurement of both the diameter of the whole BC-containing particle ($D_p$) and BC core ($D_c$). The SP2 has been used to investigate BC mixing state in China. Based on observations in urban Beijing, Liu et al. (2019a) reported that BC particles in winter exhibited larger $D_c$ and higher relative coating thickness ($D_p/D_c$) compared to those in summer, likely reflecting enhanced BC emissions from residential heating during winter. Along with the implementation of air pollution control measures in recent years, wintertime BC in Beijing showed a decreasing trend in coating thickness, with $D_p/D_c$ decreasing from $1.7 \pm 0.3$ in winter 2016 to $1.3 \pm 0.1$ in winter 2022 (Hu et al., 2025b), reflecting the substantial reduction of residential coal combustion and biomass burning emissions (Hu et al., 2025b; Pan et al., 2026; Wu et al., 2021). A recent study showed that BC with different sizes and coating thickness can be associated with different sources (Liu et al., 2023a; Zhang et al., 2020b). In addition, the evolution of BC from biomass burning has been investigated using chamber experiments and SP2 measurements, in which fire plumes from flaming and smoldering phases were introduced into a Teflon chamber under simulated atmospheric conditions, showing that the absorption efficiency of BC coatings exhibited a half-decay time of 2-3 h under light exposure (Liu et al., 2021a).

Detailed light absorption modeling using SP2 measurements ($D_p$ and $D_c$) is applied in a series of vertical measurements (e.g., aircraft and tower) over the NCP (Ding et al., 2019b; Hu et al., 2020; Kang et al., 2023; Liu et al., 2023b; Zhao et al., 2018). A vertical measurement conducted on a meteorological tower in Beijing (0-240 m) revealed that the relative coating thickness ($D_p/D_c$) increased with height under stable vertical conditions (Liu et al., 2023b). Considering the enhancement effect of BC coating on light absorption, the light absorption efficiency of BC in the PBL and free troposphere could be potentially increased by 86% and 60%, respectively (Hu et al., 2020). Based on aircraft measurements, the MAC and light absorption efficiency of BC were found to increase above clouds, because the high reflectivity of cloud top could promote the production of secondary aerosols and coatings (Liu et al., 2019b).

#### 5.1.3. Characterizing BC mixing state by SPAMS and SP-AMS

The development of single-particle analysis dates back to the 1970s with the development of surface ionization mass spectrometry, where particles were vaporized and ionized by heating metal filaments (e.g., rhenium or tungsten) (Allen et al., 2000; Noble and Prather, 1996). The SPAMS instrument employed pulsed laser ionization to analyze individual particles after they are rapidly introduced into the ionization region (Li et al., 2012). This enables simultaneous measurements of particle size and chemical composition at the single-particle level. For BC-containing particles, SPAMS can detect characteristic carbon cluster ions for freshly emitted BC, as well as identify mixed chemical components associated with aged BC. For instance, Cai et al. (2017) applied SPAMS to characterize BC particles in Beijing across different seasons, identifying major particle types including BC-OC, BC-$SO_4$, BC-$NO_3$, BC-$NO_3SO_4$, BC-NaK, BC-K, pure BC, and BC-heavy metals, with clear seasonal variations. Gong et al. (2016) applied SPAMS to analyze BC particles in Shanghai, and identified dominant contributions from traffic and biomass burning.

Besides SPAMS, the application of SP-AMS, combining SP2 with a high-resolution time-of-flight aerosol mass spectrometer (HR-ToF-AMS), enables quantitative analysis of both BC core and its coating components. The instrument employs a two-step laser process, including laser vaporization of BC followed by ionization of coating species, allowing detailed characterization of mixing composition (Onasch et al., 2012). For instance, by identifying the chemical composition of BC coating components, some studies revealed that biogenic source emissions (Zhang et al., 2026a) or open crop straw burning (Meng et al., 2024) could influence the BC mixing state, leading to enhanced light absorption by BC. Besides, Liu et al. (2019a) combined SP2 and SP-AMS measurements in Beijing, and found that small thinly coated BC particles were mainly associated with traffic emissions.

### 5.2. Modeling of BC mixing state

Numerical modeling provides a framework for understanding BC mixing state and its impacts on optical properties and climate effects. Recent studies move beyond the traditional external-internal mixing framework toward more comprehensive representations that include coating thickness, particle heterogeneity, morphology, and aging (Chen et al., 2017d; Du et al., 2025; Li et al., 2025a; Shen et al., 2026; Zhang et al., 2026b). These developments highlight that BC absorption is not only controlled by coating presence, but also by its distribution, composition, and particle-to-particle variability, which can significantly enhance light absorption and contribute to biases in global models (Chen et al., 2025; Liu et al., 2017). A key advance is the development of unified theoretical frameworks linking BC mixing state (coating-thickness distributions) and absorption enhancement, enabling more physically consistent representations in chemical transport models (Wang et al., 2023b). In parallel, observation-constrained optical parameterizations incorporating mixing state, non-sphericity, and heterogeneity have been developed, improving BC absorption estimates and reducing biases in traditional models (Chen et al., 2023a, 2024).

The BC mixing state modeling has been carried out in China. A few examples are given here. In the BTH region, Du et al. (2025) explicitly represented BC coating structures and found that simulated absorption enhancement at 880 nm decreased by approximately 30-43% compared with simplified schemes, bringing results closer to observations. Similarly, in the YRD, Yin et al. (2024) introduced a source- and age-resolved framework, showing that source type and aging state alter optical properties of BC and reduce the overestimation of its mass absorption cross section and direct radiative forcing. Other studies have further demonstrated that assumptions about BC mixing state can influence the regional radiation balance and photochemical processes, including near-surface ozone formation (An et al., 2021).

Beyond optical effects, modeling studies also highlight the critical role of mixing state in governing BC atmospheric lifecycle and removal processes. Progressive aging increases BC hygroscopicity, facilitating its activation as CCN and enhancing wet scavenging efficiency (Ding et al., 2019c; Zhang et al., 2025d). Recent simulations incorporating explicit BC aging schemes (e.g., WRF-CMAQ) suggested that emission control policies in China have not only reduced BC concentrations but also altered its mixing state, with a significant decline in the fraction of thickly coated BC particles from 2013 to 2019. Furthermore, emerging ML-based parameterizations (e.g., Community Atmosphere Model version 6 with the four-mode Modal Aerosol Module and machine learning, CAM6-MAM4-ML) provide a promising pathway to efficiently represent BC aging and mixing processes in global climate models, helping reduce uncertainties in aerosol-climate interactions (Shen et al., 2024a).

Currently, the integration of observational evidence and modeling frameworks for BC mixing state is still at an early stage. Future work should prioritize the systematic incorporation of observation-constrained mixing-state characteristics into model parameterizations, as well as the development of unified frameworks that can capture the dynamic evolution, source dependence, and heterogeneity of BC in the real atmosphere. Such efforts are essential for reducing uncertainties in both climate forcing estimates and health impact assessments of BC.

## 6. Health effects of BC

As a characteristic product from incomplete combustion of biomass and fossil fuels, BC has a graphitic carbon core with a fractal structure, a large specific surface area, and strong adsorption capacity, making it a “mobile carrier” of toxic pollutants (Chen et al., 2023d; Dhada et al., 2025; Li et al., 2019). The health effects of atmospheric BC have been

widely investigated through both laboratory and epidemiological studies.

Upon inhalation, BC can induce excessive production of reactive oxygen species (ROS), leading to oxidative stress by disrupting the balance between oxidant generation and antioxidant defenses (Niranjan and Thakur, 2017; Tang et al., 2024b). The generated ROS can attack biological macromolecules such as lipids, proteins, and DNA, altering their structure and function before ultimately damaging cells and tissues (Niranjan and Thakur, 2017; Xu et al., 2022). Oxidative stress also activates redox-sensitive signaling pathways, including nuclear factor κB (NF-κB), promoting inflammatory responses through the release of cytokines and chemokines (Al-Kindi et al., 2020; Brook et al., 2017). In addition, environmentally persistent free radicals (EPFRs) associated with BC particles can further catalyze ROS production, prolonging oxidative stress in biological environments (Tang et al., 2024b; Yang et al., 2025b). These mechanisms collectively contribute to a range of adverse health outcomes, including respiratory symptoms, cardiovascular diseases, and increased cancer risks. Fig. 7 provides examples of studies linking BC mass, BC sources, and BC mixing states to health outcomes in China.

### 6.1. BC as one of the major health-risk components in $PM_{2.5}$

#### 6.1.1. Cytotoxicity evidence of BC

The fine size of BC particles enables prolonged atmospheric suspension and efficient inhalation, with deposition occurring throughout the respiratory tract. Such exposure has been linked to a variety of serious health effects, encompassing both cardiopulmonary and neurological impairments (Chen et al., 2026; Roy et al., 2024). Oxidative stress represents one of the core pathways of BC-induced chemical toxicity (Kuang et al., 2020; Zhu et al., 2020). *In vitro* exposure studies consistently demonstrate that BC induces dose-dependent ROS generation, thereby triggering inflammatory responses and cytotoxicity. The toxic profile of BC is not solely attributable to its carbonaceous core but is synergistically amplified by co-adsorbed hazardous components, including PAHs and transition metals (e.g., chromium, nickel, cadmium) that can induce ROS production. Studies have shown that inhaling BC could promote lung carcinogenesis through ROS-mediated oxidative stress and inflammatory responses (Niranjan and Thakur, 2017; Zimmermann, 2015).

Furthermore, ultrafine BC particles (<100 nm) possess strong biological barrier-penetrating ability, and they can cross the blood-brain barrier and placental barrier to initiate DNA damage. At the molecular level, BC can trigger DNA strand breaks, abnormal methylation, and histone modifications through AhR, TLR, and other receptor-mediated pathways (Niranjan and Thakur, 2017; Nze-Dike et al., 2025). It can also interfere with miRNA expression, inducing oxidative stress and inflammation and significantly increasing carcinogenic risk (Niranjan and Thakur, 2017; Nze-Dike et al., 2025). Collectively, these genotoxic and epigenomic alterations can reshape gene expression profiles, disrupt cellular homeostasis, and ultimately drive malignant transformation. Given its capacity to induce persistent molecular changes even at low exposure doses, BC is increasingly recognized as a long-acting atmospheric pollutant with sustained adverse health consequences.

#### 6.1.2. In vivo evidence of BC toxicity

*In vivo* studies are essential for elucidating the biodistribution, translocation, and multi-organ effects of BC, which cannot be fully captured by *in vitro* systems. These studies have provided critical evidence for systemic toxicity beyond the initial pulmonary response. Studies have shown that BC can penetrate the alveolar barrier in a monodisperse state, evade hepatic surveillance via lymphatic and systemic circulation, and specifically accumulate in lung-associated lymph nodes (LALN) and the spleen, forming a unique translocation pathway. These findings provide direct evidence for the connection between local pulmonary injury and systemic toxicity (Chu et al., 2018; Kim et al., 2025; Kleinman et al., 2000). BC can also induce oxidative stress and

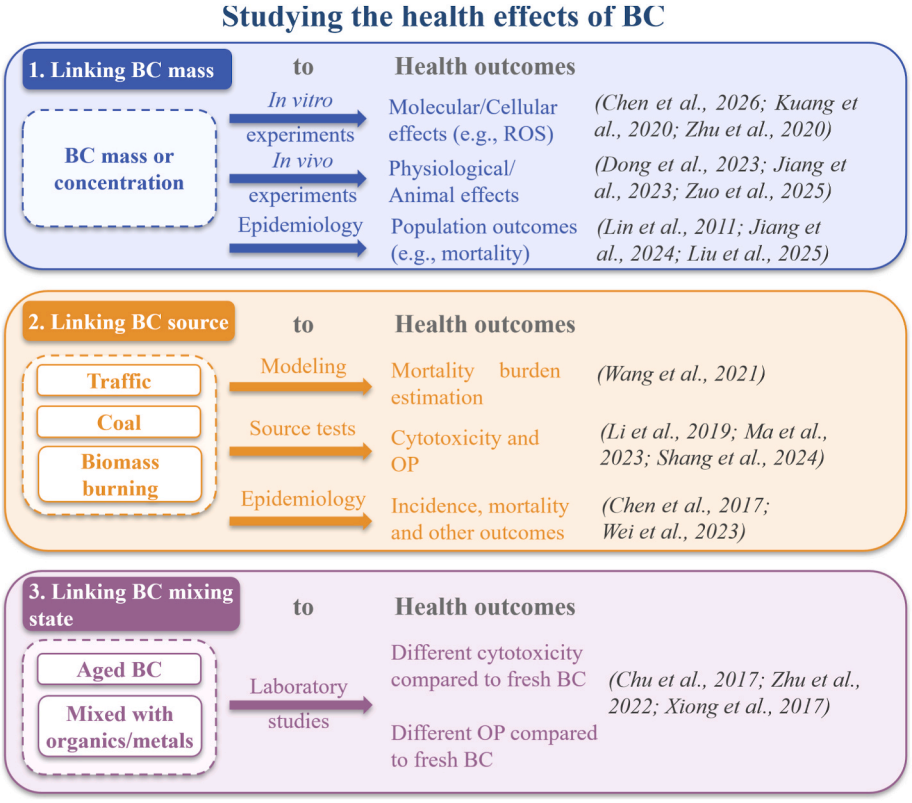


**Fig. 7.** Examples of studies linking BC mass, BC sources, and BC mixing states to health outcomes in China. Details are provided in Sections 6.1, 6.2, and 6.3.

protein misfolding, downregulate myocardial Hsp70 expression, activate inflammatory factors (e.g., IL-1β and IL-6), and cause cardiac inflammatory injury (Zuo et al., 2025). In addition to direct toxic effects, BC may also exert indirect health impacts by serving as a carrier for other pathogenic agents. In a study investigating respiratory viral replication, Dong et al. (2023) observed that inhaled BC particles are able to increase the occurrence and severity of respiratory virus infection by delivering the virus deep into the respiratory tract and distant organs of BALB/c mice. Existing *in vivo* evidence has also demonstrated the more significant toxicity of oxidized BC. Pregnant mice exposed to oxidized BC exhibited impaired spermatogenic function in male offspring (Jiang et al., 2023). In C57BL/6 mice, heterogeneous ozone-aged oxidized BC triggered elevated pulmonary inflammatory cytokines, with lung injury mediated by the IL-33 signaling pathway and related cascades (Chu et al., 2016, 2018). These findings reveal specific *in vivo* toxic mechanisms of BC exposure, providing key explanations for the associations between BC and health outcomes (Zhang et al., 2022b).

#### 6.1.3. Epidemiological evidence of BC effects

Early time-series studies reported significant associations between ambient BC concentrations and mortality outcomes, including respiratory mortality observed in Barcelona (Ballester et al., 1996). Evidence from the American Cancer Society cohort indicated that long-term BC exposure was significantly associated with increased respiratory mortality (Smith et al., 2009). These epidemiological findings are consistent with the physicochemical properties of BC particles, which possess large surface areas capable of adsorbing toxic co-emitted substances such as PAHs and metals that can promote oxidative stress and inflammatory responses (Chen et al., 2023d; Dhada et al., 2025; Li et al., 2019). The small particle size of BC also facilitates deep penetration into the respiratory tract and potential translocation into the bloodstream, thereby contributing to systemic health effects (Chen et al., 2026; Roy et al., 2024). As a result, in the 2021 Global Air Quality Guidelines, the World Health Organization identified carbonaceous aerosols, including BC, as components of particular health concern, based on a systematic review of epidemiological and toxicological evidence (World Health Organization, 2021).

In China, a growing number of large-scale epidemiological studies have identified that BC is the major health-risk component in $PM_{2.5}$. Multi-city analyses covering hundreds of Chinese cities have shown that short-term exposure to BC was significantly associated with increased hospital admissions for cardiovascular diseases, with effect estimates exceeding those of several other major $PM_{2.5}$ components (Tian et al., 2024). Similarly, nationwide case-crossover studies have reported significant associations between BC exposure and the onset of acute coronary syndrome, with BC contributing substantially to the joint effects of multiple $PM_{2.5}$ components (Jiang et al., 2024). Long-term cohort analyses have further indicated that BC exposure was linked to elevated risks of several cancers, including gastrointestinal and lung cancer. Advanced mixture analyses (e.g., weighted quantile sum regression), which address the high correlations among $PM_{2.5}$ components, consistently rank BC as one of the most influential constituents driving adverse health outcomes (Hu et al., 2025a; Yang et al., 2024). Nationwide evaluations of the Air Pollution Prevention and Control Action Plan have further demonstrated that reductions in BC concentrations were associated with a substantial decrease in hospital admissions across multiple disease categories (Liu et al., 2025a). The above findings highlight the important role of BC in adverse health effects of $PM_{2.5}$ pollution in China.

A number of epidemiological studies conducted in China have further quantified the exposure-response relationships between BC concentration and a wide range of health outcomes. These studies employed different study designs, such as time-series analyses (Chen et al., 2022; Geng et al., 2013; Hua et al., 2014), prospective cohort studies (Gan et al., 2013; Li et al., 2022a), and panel studies (Lin et al., 2011; Xu et al., 2022), with exposure assessment based on fixed-site monitoring (Lin et al., 2011; Xu et al., 2022), chemical transport models (Guo et al., 2022), or gridded datasets of BC concentrations (Han et al., 2023; Zhang et al., 2022a). The reported health outcomes span multiple disease categories, including respiratory (Chen et al., 2022; Gan et al., 2013; Hua et al., 2014; Lin et al., 2011), cardiovascular (Geng et al., 2013; Peng et al., 2009; Xu et al., 2022) and neurological outcomes (Chen et al., 2017c; Li et al., 2022a; Zhang et al., 2022a). Based on the exposure-response relationships, recent studies have further incorporated BC-specific risk estimates into models to quantify the disease burden attributable to BC exposure in China (Cui et al., 2022; Wang et al., 2021b; Zhao et al., 2024b). The above epidemiological evidence indicates that BC is a major contributor to $PM_{2.5}$-attributable health risks.

### 6.2. Health effects of BC from different sources

BC particles emitted from specific sources exhibit substantial differences in their physicochemical properties, which may lead to different health effects. Biomass and coal combustion under relatively low-temperature conditions typically generate substantial fractions of char-like BC, whereas diesel engines operating at higher temperatures produce more graphitized soot particles (Han et al., 2022; Shrestha et al., 2010). These particles also differ in size and chemical composition. Traffic-derived BC generally exhibits smaller particle sizes compared with biomass- and coal-derived BC, which may facilitate deeper penetration into the respiratory tract and higher deposition efficiency in the human body (Liu et al., 2023a; Zhang et al., 2020b). In addition to particle size differences, source-specific variations are also reflected in chemical composition. BC from biomass burning is found to be associated with oxygenated organic compounds and is characterized by higher O/C ratios than traffic-derived BC (Cai et al., 2023; Sha et al., 2021). These source-specific physicochemical properties can further influence oxidative potential (OP) and cellular inflammatory responses, suggesting that BC from different sources may exhibit substantially different toxic effects even at the same mass concentrations.

Several approaches have been applied to investigate the source-specific health effects of BC, including atmospheric modeling, toxicological experiments, and source-specific emission tests. Modeling studies have quantified the disease burden attributable to BC emissions from different sectors. For instance, global simulations have identified residential combustion as a major contributor to BC-attributable mortality worldwide, while regional modeling in China using the CMAQ model has highlighted industrial and residential emissions as major contributors (Chowdhury et al., 2022; Wang et al., 2021b). However, these modeling approaches generally assume equal toxicity across BC sources. Toxicological studies provide complementary evidence by directly comparing the biological responses induced by BC from different sources. Nevertheless, laboratory studies often rely on particles collected on filters, and sample extraction or processing may modify the surface coatings and chemical composition of BC particles (Li et al., 2019; Ma et al., 2023; Shang et al., 2024), making it difficult to fully represent real atmospheric exposures. Experimental comparisons of emissions from diesel engines, biomass burning, and coal combustion have suggested that diesel-derived BC exhibits higher OP, partly due to its smaller particle size and higher abundance of reactive surface sites (Li et al., 2019; Ma et al., 2023).

Epidemiological studies based on ambient observations can provide relatively direct population-level evidence for heterogeneous health effects of BC from different sources. However, such studies remain limited. A population-based cohort study reported that individuals living within 50 m of major roadways had approximately 7% higher risk of dementia than those residing more than 300 m away (Chen et al., 2017c), which may partly reflect higher exposure to traffic-related BC and co-emitted pollutants. Similarly, a panel study conducted in rural southwestern China found that BC exposure was strongly associated with elevated systolic blood pressure, with larger effects observed

among women living closer to highways where motor vehicle emissions contribute additional BC exposure (Baumgartner et al., 2014). Besides BC from traffic emission, another important source of BC in recent years is wildfire. Studies have shown that between 2010 and 2020, BC emissions in the western United States increased by 86% due to wildfires, which has been associated with an estimated 670 premature deaths annually (Wei et al., 2023b). Long-range transport of wildfire emissions has been shown to influence air quality in the NCP (Zhang et al., 2025b). An epidemiological study investigated the association between BC sources (traffic and residential combustion sources) and stroke incidence (Ljungman et al., 2019). Further studies are still needed to identify BC sources with higher health risks in specific regions or areas.

### 6.3. Health effects of BC with different mixing states

Fresh BC is typically emitted as externally mixed particles. During atmospheric transport, these particles are gradually coated by other species and become internally mixed (Tan et al., 2020). Such aging processes can significantly alter the physicochemical properties and toxicity of BC (Cai et al., 2023; Sha et al., 2021). Laboratory studies suggest that aged BC exhibits stronger biological effects than freshly emitted particles. For instance, BC coated with PAHs induces higher mortality in lung macrophages (Chu et al., 2017; Misaki et al., 2021), while BC associated with heavy metals, such as Pb, can stimulate elevated expression levels of inflammatory cytokines in bronchial epithelial cells (Jiang et al., 2018). Atmospheric oxidation processes further modify BC toxicity. Under visible light irradiation, BC particles can mediate the generation of ROS, including superoxide anions and hydroxyl radicals, which can oxidize surface-bound organic species, thereby enhancing OP and cytotoxicity (Jiang et al., 2023; Zhu et al., 2022). $O_3$ aging on BC has been shown to increase the OP of BC and induce stronger pulmonary inflammatory responses both *in vivo* and *in vitro* (Chu et al., 2016; Zhu et al., 2020).

Among the species mixed with BC, organic compounds appear to play a key role in modulating toxicity. Several organic species, including PAHs, humic-like substances (HULIS), and quinones, have been associated with inflammatory responses in epidemiological and experimental studies (Jiang et al., 2021; Kim et al., 2013; Peng et al., 2023a). Laboratory studies further demonstrate that organic coatings can enhance BC toxicity. For instance, controlled exposure experiments showed that hydrocarbons coated on BC particles significantly enhanced cytotoxicity in human lung epithelial cells (Hakkarainen et al., 2022), whereas quinone-coated BC induced stronger pulmonary inflammation in mice than uncoated BC (Chu et al., 2017). Quinones are also key contributors to particle OP and can interact with transition metals to promote rapid ROS generation (Misaki et al., 2021).

Transition metals, including Cu, Mn, and Fe, could catalyze ROS generation and enhance OP, thereby promoting inflammatory responses (Karavalakis et al., 2017; McWhinney et al., 2013). Experimental studies showed that complexation of metals on BC surfaces can substantially alter oxidative potential, highlighting their catalytic role in ROS production (Li et al., 2019; Ma et al., 2023). Quinones and iron can synergistically generate hydroxyl radicals via redox cycling processes, further amplifying particle toxicity (Xiong et al., 2017). Beyond modifying intrinsic toxicity, atmospheric aging also alters the hygroscopicity and size of BC particles, which can influence their deposition within the human respiratory system. A recent modeling study showed that neglecting mixing states may underestimate deposited BC mass in respiratory regions by approximately 5-15% (Ching et al., 2020). These findings indicate that neglecting BC mixing states may introduce biases in both toxicity characterization and exposure assessment in health studies.

## 7. Future perspectives

Despite substantial progress made in recent years in understanding the environmental and health impacts of BC in China, several critical knowledge gaps remain that warrant further investigation, including:

(1) Standardization of BC measurement methods: In China, optical-based methods, particularly filter-based instruments such as the AE33, are extensively applied for BC concentration measurements. However, discrepancies between in-situ and filter-based methods have revealed inconsistencies across different instruments and approaches, introducing uncertainties in BC quantification. These discrepancies are further amplified for aged BC with higher Ångström exponents. Therefore, developing unified and traceable calibration standards, particularly for filter-based techniques that are susceptible to measurement artifacts, is essential for improving data reliability and minimizing discrepancies across studies. International initiatives, such as Europe's stanBC project, offer valuable standards, and similar efforts should be prioritized or adapted in China;

(2) Validation of gridded BC datasets: Emerging gridded BC datasets developed in China, such as CAQRA-aerosol, TAP, and CHAP, have been widely applied in BC trend analysis, policy evaluation, and health effect assessment. However, these datasets show discrepancies that vary regionally, highlighting the need for further evaluation against long-term ground-based observations. A more comprehensive understanding of BC datasets is essential for quantifying uncertainties associated with different products and for selecting the most appropriate dataset for a given region or area;

(3) Integration of observation and atmospheric modeling: Critical needs lie in the integration of observational data and atmospheric models (e.g., GEOS-Chem or WRF/CMAQ) to better characterize BC sources and mixing states in China. Key priorities include refining emission inventories for underrepresented Chinese sources (residential solid fuel, fireworks, coke/brick production). In China, nitrate-driven aging is particularly important due to high $NO_x$ and $NH_3$ levels during haze periods. Notably, some typical sources in China may emit BC already mixed with other components, suggesting that aging can begin from partially coated rather than bare particles. These processes alter BC mixing state, hygroscopicity, atmospheric lifetime, scavenging, and optical properties. Therefore, to reduce uncertainties in source, transport, and climate effect estimates, China-specific aging parameterizations should be developed by integrating multi-site observations, laboratory experiments, and modeling;

(4) Investigation of BC health effects: While previous control policies in China have substantially reduced BC mass concentrations, the next mitigation stage must move beyond bulk reductions to identify high-risk BC sources. This is particularly important because BC has been consistently identified as one of the most health-relevant components of $PM_{2.5}$, with robust associations with multiple adverse health outcomes, including cardiovascular, respiratory, and neurological diseases. Future studies should also explore the health effects of BC during atmospheric aging, especially under typical pollution conditions in China. Epidemiological studies should focus on individual-level exposure and use multi-omics approaches to characterize BC-related biological response pathways. Given China's large and socioeconomically diverse population, establishing urban-rural gradient exposure cohorts would help systematically quantify combined indoor and outdoor BC exposure among residents. Integrating sensors and satellite remote sensing would be helpful in investigating personal BC exposure risks among different vulnerable populations nationwide.

## CRediT authorship contribution statement

**Qi Zhou:** Data curation, Formal analysis, Investigation, Visualization, Writing – original draft. **Shunyao Wang:** Investigation, Writing –

review & editing. **Shujun Bie:** Investigation, Writing – review & editing. **Junjie Cai:** Investigation, Writing – review & editing. **Yingjun Chen:** Investigation, Writing – review & editing. **Yuan Cheng:** Investigation. **Xiang Ding:** Investigation. **Jianwei Gu:** Investigation, Writing – review & editing. **Jie Li:** Investigation. **Weijun Li:** Investigation, Writing – review & editing. **Dantong Liu:** Investigation, Writing – review & editing. **Jiaying Liu:** Investigation, Writing – review & editing. **Yue Liu:** Investigation, Writing – review & editing. **Jing Shang:** Investigation, Writing – review & editing. **Xiao Tang:** Investigation, Writing – review & editing. **Rui Tang:** Investigation, Writing – review & editing. **Yingze Tian:** Investigation, Writing – review & editing. **Jiandong Wang:** Investigation, Writing – review & editing. **Shuxiao Wang:** Investigation. **Jing Wei:** Investigation, Writing – review & editing. **Yi Wei:** Investigation, Writing – review & editing. **Yaxin Xiang:** Investigation. **Caiqing Yan:** Investigation, Writing – review & editing. **Fenfen Zhang:** Investigation, Writing – review & editing. **Zhouyang Zhang:** Investigation, Writing – review & editing. **Gan Zhang:** Investigation, Writing – review & editing. **Qiang Zhang:** Investigation. **Yan Zhang:** Investigation, Writing – review & editing. **Guangcai Zhong:** Investigation, Writing – review & editing. **Mei Zheng:** Conceptualization, Funding acquisition, Investigation, Supervision, Writing – review & editing.

## Declaration of competing interests

The authors declare that they have no known competing financial interests or personal relationships that could have appeared to influence the work reported in this paper.

## Acknowledgments

This study was supported by the Jing-Jin-Ji Regional Integrated Environmental Improvement-National Science and Technology Major Project (No. 2025ZD1204800). We are grateful to Dr. Tianle Zhang for providing valuable and helpful comments for improving this manuscript.

## Data availability

Data will be made available on request.

## References

Adachi, K., Chung, S.H., Buseck, P.R., 2010. Shapes of soot aerosol particles and implications for their effects on climate. J. Geophys. Res. 115, D15206.
Aklilu, Y.A., Michelangeli, D.V., 2004. Box model investigation of the effect of soot particles on ozone downwind from an urban area through heterogeneous reactions. Environ. Sci. Technol. 38, 5540–5547.
Al-Kindi, S.G., Brook, R.D., Biswal, S., Rajagopalan, S., 2020. Environmental determinants of cardiovascular disease: lessons learned from air pollution. Nat. Rev. Cardiol. 17, 656–672.
Ali, M.U., Lin, S., Yousaf, B., Abbas, Q., Hameed, R., Zheng, C., Kuang, X., Wong, M., 2021. Emission sources and full spectrum of health impacts of black carbon associated polycyclic aromatic hydrocarbons (PAHs) in urban environment: a review. Crit. Rev. Environ. Sci. Technol. 51, 857–896.
Allen, J.O., Fergenson, D.P., Gard, E.E., Hughes, L.S., Morrical, B.D., Kleeman, M.J., Gross, D.S., Gälli, M.E., Prather, K.A., Cass, G.R., 2000. Particle detection efficiencies of aerosol time of flight mass spectrometers under ambient sampling conditions. Environ. Sci. Technol. 34, 211–217.
An, J., Lv, H., Xue, M., Zhang, Z., Hu, B., Wang, J., Zhu, B., 2021. Analysis of the effect of optical properties of black carbon on ozone in an urban environment at the Yangtze River Delta, China. Adv. Atmos. Sci. 38, 1153–1164.
Andreae, M.O., Gelencser, A., 2006. Black carbon or brown carbon? The nature of light-absorbing carbonaceous aerosols. Atmos. Chem. Phys. 6, 18.
Asmi, E., Sipkens, T.A., Saturno, J., Backman, J., Vasilatou, K., Weingartner, E., Keller, A., Ciupek, K., Müller, T., Babu Suja, A., Močnik, G., Drinovec, L., Eleftheriadis, K., Gini, M.I., Nowak, A., Corbin, J.C., 2025. Mass absorption cross-section of ambient black carbon aerosols - a review. npj Clim. Atmos. Sci. 9, 17.
Atribak, I., Bueno-López, A., García-García, A., 2010. Uncatalysed and catalysed soot combustion under $NO_x + O^2$: real diesel versus model soots. Combust. Flame 157, 2086–2094.
Ballester, F., Corella, D., Pérez-Hoyos, S., Hervás, A., 1996. Air pollution and mortality in Valencia, Spain: a study using the APHEA methodology. J. Epidemiol. Community Health 50, 527–533.
Baumgartner, J., Zhang, Y., Schauer, J., Huang, W., Wang, Y., Ezzati, M., 2014. Highway proximity and black carbon from cookstoves as a risk factor for higher blood pressure in rural China. Proc. Natl. Acad. Sci. USA 111, 13229–13234.
Bond, T.C., Doherty, S.J., Fahey, D.W., Forster, P.M., Berntsen, T., DeAngelo, B.J., Flanner, M.G., Ghan, S., Kaercher, B., Koch, D., Kinne, S., Kondo, Y., Quinn, P.K., Sarofim, M.C., Schultz, M.G., Schulz, M., Venkataraman, C., Zhang, H., Zhang, S., Bellouin, N., et al., 2013. Bounding the role of black carbon in the climate system: a scientific assessment. J. Geophys. Res. Atmos. 118, 5380–5552.
Briggs, N.L., Long, C.M., 2016. Critical review of black carbon and elemental carbon source apportionment in Europe and the United States. Atmos. Environ. 144, 409–427.
Brook, R.D., Newby, D.E., Rajagopalan, S., 2017. Air pollution and cardiometabolic disease: an update and call for clinical trials. Am. J. Hypertens. 31, 1–10.
Cai, J., Chen, Y., Zeng, J., Jiang, H., Han, Y., Cui, M., Peng, Y., Liu, Z., Zhang, G., Chen, J., 2026a. Physicochemical properties and aging behavior of black carbon across emission sources determined by char and soot subgroups. Environ. Sci. Technol. 10, 8018–8028.
Cai, J., Jiang, H., Chen, Y., Liu, Z., Han, Y., Shen, H., Song, J., Li, J., Zhang, Y., Wang, R., Chen, J., Zhang, G., 2023. Char dominates black carbon aerosol emission and its historic reduction in China. Nat. Commun. 14, 6444.
Cai, J., Wang, J., Zhang, Y., Tian, H., Zhu, C., Gross, D.S., Hu, M., Hao, J., He, K., Wang, S., Zheng, M., 2017. Source apportionment of Pb-containing particles in Beijing during January 2013. Environ. Pollut. 226, 30–40.
Cai, J., Wu, J., Chen, Y., 2025. Characterization of freshly-emitted particles from poplar wood burning: OC/EC, morphology, and elemental analysis under varying ignition temperatures. Atmos. Environ. 355, 121271.
Cai, J., Zeng, J., Chen, Y., Ma, H., Jiang, H., Peng, Y., Cao, F., Han, Y., Liu, Z., Feng, X., 2026b. Evolution of single-particle morphology and composition from typical bituminous coal combustion under different temperatures. Atmos. Environ. 374, 121875.
Cao, F., Zhang, Y., Ren, L., Liu, J., Li, J., Zhang, G., Liu, D., Sun, Y., Wang, Z., Shi, Z., Fu, P., 2017. New insights into the sources and formation of carbonaceous aerosols in China: potential applications of dual-carbon isotopes. Natl. Sci. Rev. 4, 804–806.
Cao, G., Zhang, X., Zheng, F., 2006. Inventory of black carbon and organic carbon emissions from China. Atmos. Environ. 40, 6516–6527.
Champion, W.M., Charley, P.H., Klein, B., Stewart, K., Solomon, P.A., Montoya, L.D., 2017a. Perception, culture, and science: a framework to identify in-home heating options to improve indoor air quality in the Navajo Nation. Sci. Total Environ. 580, 297–306.
Champion, W.M., Connors, L., Montoya, L.D., 2017b. Emission factors of fine particulate matter, organic and elemental carbon, carbon monoxide, and carbon dioxide for four solid fuels commonly used in residential heating by the US Navajo Nation. J. Air Waste Manage. Assoc. 67, 1020–1035.
Chen, B., Andersson, A., Lee, M., Kirillova, E.N., Xiao, Q., Kruså, M., Shi, M., Hu, K., Lu, Z., Streets, D.G., Du, K., Gustafsson, Ö., 2013. Source forensics of black carbon aerosols from China. Environ. Sci. Technol. 47, 9102–9108.
Chen, B., Bai, Z., Cui, X., Chen, J., Andersson, A., Gustafsson, Ö., 2017a. Light absorption enhancement of black carbon from urban haze in Northern China winter. Environ. Pollut. 221, 418–426.
Chen, D., Wang, X., Li, Y., Lang, J., Zhou, Y., Guo, X., Zhao, Y., 2017b. High-spatiotemporal-resolution ship emission inventory of China based on AIS data in 2014. Sci. Total Environ. 609, 776–787.
Chen, G., Liu, C., Wang, J., Yin, Y., Wang, Y., 2024. Accounting for black carbon mixing state, nonsphericity, and heterogeneity effects in its optical property parameterization in a climate model. J. Geophys. Res. Atmos. 129 e2024JD041135.
Chen, G., Wang, J., Wang, Y., Wang, J., Jin, Y., Cheng, Y., Yin, Y., Liao, H., Ding, A., Wang, S., Hao, J., Liu, C., 2023a. An aerosol optical module with observation-constrained black carbon properties for global climate models. J. Adv. Model. Earth Syst. 15 e2022MS003501.
Chen, H., Kwong, J.C., Copes, R., Tu, K., Villeneuve, P.J., van Donkelaar, A., Hystad, P., Martin, R.V., Murray, B.J., Jessiman, B., Wilton, A.S., Kopp, A., Burnett, R.T., 2017c. Living near major roads and the incidence of dementia, Parkinson's disease, and multiple sclerosis: a population-based cohort study. Lancet 389, 718–726.
Chen, J., Yu, W., Cui, X., Zhang, Q., Li, T., Wang, X., Ren, Y., Wang, H., Wang, Q., 2026. Black carbon in urban Jinan: variations, health risks, and driving factors analyzed with machine learning. J. Environ. Sci. 160, 508–516.
Chen, L., Gao, Y., Zhang, M., Fu, J., Zhu, J., Liao, H., Li, J., Huang, K., Ge, B., Wang, X., Lam, Y., Lin, C., Itahashi, S., Nagashima, T., Kajino, M., Yamaji, K., Wang, Z., Kurokawa, J., 2019. MICS-ASIA III: Multi-model comparison and evaluation of aerosol over East Asia. Atmos. Chem. Phys. 19, 11911–11937.
Chen, S., Wang, Q., Zhang, Y., Tian, J., Wang, J., Ho, S.S.H., Li, L., Ran, W., Han, Y., Pavese, G., Cao, J., 2023b. Heterogeneous characteristics and absorption enhancement of refractory black carbon in an urban city of China. Sci. Total Environ. 879, 162997.
Chen, T., Norback, D., Deng, Q., Huang, C., Qian, H., Zhang, X., Sun, Y., Wang, T., Zhang, Y., Li, B., Kan, H., Wei, L., Liu, C., Xu, Y., Zhao, Z., 2022. Maternal exposure to $PM_{2.5}$/BC during pregnancy predisposes children to allergic rhinitis which varies by regions and exclusive breastfeeding. Environ. Int. 165, 107315.
Chen, X., Ching, J., Wu, F., Matsui, H., Jacobson, M.Z., Zhang, F., Wang, Y., Zhang, Z., Liu, D., Zhu, S., Rudich, Y., Shi, Z., Yoo, H., Jeon, K.J., Li, W., 2025. Locating the missing absorption enhancement due to multi-core black carbon aerosols. Nat. Commun. 16, 10187.
Chen, X., Wang, Z., Yu, F., Pan, X., Li, J., Ge, B., Wang, Z., Hu, M., Yang, W., Chen, H., 2017d. Estimation of atmospheric aging time of black carbon particles in the polluted atmosphere over central-eastern China using microphysical process analysis in regional chemical transport model. Atmos. Environ. 163, 44–56.

Chen, X., Ye, C., Wang, Y., Wu, Z., Zhu, T., Zhang, F., Ding, X., Shi, Z., Zheng, Z., Li, W., 2023c. Quantifying evolution of soot mixing state from transboundary transport of biomass burning emissions. iScience 26, 108125.
Chen, Y., Cai, W., Huang, G., Li, J., Zhang, G., 2012. Stable carbon isotope of black carbon from typical emission sources in China. Huanjing Kexue 33, 673–678.
Chen, Y., Cheng, Y., Hsu, C., 2023d. Characterization of the sources and health risks of polycyclic aromatic hydrocarbons in $PM_{2.5}$ and their relationship with black carbon: a case study in northern Taiwan. Environ. Pollut. 336, 122427.
Chen, Y., Sheng, G., Bi, X., Feng, Y., Mai, B., Fu, J., 2005. Emission factors for carbonaceous particles and polycyclic aromatic hydrocarbons from residential coal combustion in China. Environ. Sci. Technol. 39, 1861–1867.
Chen, Y., Zhi, G., Feng, Y., Fu, J., Feng, J., Sheng, G., Simoneit, B.R.T., 2006. Measurements of emission factors for primary carbonaceous particles from residential raw-coal combustion in China. Geophys. Res. Lett. 33, L20815.
Chen, Y., Zhi, G., Feng, Y., Liu, D., Zhang, G., Li, J., Sheng, G., Fu, J., 2009. Measurements of black and organic carbon emission factors for household coal combustion in China: implication for emission reduction. Environ. Sci. Technol. 43, 9495–9500.
China, S., Mazzoleni, C., Gorkowski, K., Aiken, A.C., Dubey, M.K., 2013. Morphology and mixing state of individual freshly emitted wildfire carbonaceous particles. Nat. Commun. 4, 2122.
Ching, J., Kajino, M., Matsui, H., 2020. Resolving aerosol mixing state increases accuracy of black carbon respiratory deposition estimates. One Earth 3, 763–776.
Chowdhury, S., Pozzer, A., Haines, A., Klingmueller, K., Muenzel, T., Paasonen, P., Sharma, A., Venkataraman, C., Lelieveld, J., 2022. Global health burden of ambient $PM_{2.5}$ and the contribution of anthropogenic black carbon and organic aerosols. Environ. Int. 159, 107020.
Chu, H., Hao, W., Cheng, Z., Huang, Y., Wang, S., Shang, J., Hou, X., Meng, Q., Zhang, Q., Jia, L., Zhou, W., Wang, P., Jia, G., Zhu, T., Wei, X., 2018. Black carbon particles and ozone-oxidized black carbon particles induced lung damage in mice through an interleukin-33 dependent pathway. Sci. Total Environ. 644, 217–228.
Chu, H., Shang, J., Jin, M., Chen, Y., Pan, Y., Li, Y., Tao, X., Cheng, Z., Meng, Q., Li, Q., Jia, G., Zhu, T., Hao, W., Wei, X., 2017. Comparison of lung damage in mice exposed to black carbon particles and 1,4-naphthoquinone coated black carbon particles. Sci. Total Environ. 580, 572–581.
Chu, H., Shang, J., Jin, M., Li, Q., Chen, Y., Huang, H., Li, Y., Pan, Y., Tao, X., Cheng, Z., Meng, Q., Jia, G., Zhu, T., Wei, X., Hao, W., 2016. Comparison of lung damage in mice exposed to black carbon particles and ozone-oxidized black carbon particles. Sci. Total Environ. 573, 303–312.
Chughtai, A.R., Kim, J.M., Smith, D.M., 2002. The effect of air/fuel ratio on properties and reactivity of combustion soots. J. Atmos. Chem. 43, 21–43.
Chughtai, A.R., Smith, D.M., 1994. The surface-structure and reactivity of black carbon. Abstr. Pap. Am. Chem. Soc. 208, 49–COLL.
Crippa, M., Guizzardi, D., Pagani, F., Schiavina, M., Melchiorri, M., Pisoni, E., Graziosi, F., Muntean, M., Maes, J., Dijkstra, L., Van Damme, M., Clarisse, L., Coheur, P., 2024. Insights into the spatial distribution of global, national, and subnational greenhouse gas emissions in the emissions database for global atmospheric research (EDGAR v8.0). Earth Syst. Sci. Data 16, 2811–2830.
Cui, C., Liu, Y., Chen, L., Liang, S., Shan, M., Zhao, J., Liu, Y., Yu, S., Sun, Y., Mao, J., Zhang, H., Gao, S., Ma, Z., 2022. Assessing public health and economic loss associated with black carbon exposure using monitoring and MERRA-2 data. Environ. Pollut. 313, 120190.
Cui, M., Xu, Y., Yu, B., Yan, C., Li, J., Zheng, M., Chen, Y., 2023b. Characterization of carbonaceous matter emitted from residential coal and biomass combustion by experimental simulation. Atmos. Environ. 293, 119447.
Cui, M., Xu, Y., Zhang, F., Yan, C., Li, J., Zheng, M., Chen, Y., 2023a. Real-world characterization of carbonaceous substances from industrial stationary and process source emissions. Sci. Total Environ. 854, 158505.
Cui, X., Wang, X., Yang, L., Chen, B., Chen, J., Andersson, A., Gustafsson, Ö., 2016. Radiative absorption enhancement from coatings on black carbon aerosols. Sci. Total Environ. 551–552, 51–56.
Currie, L.A., Benner Jr., B.A., Kessler, J.D., Klinedinst, D.B., Klouda, G.A., Marolf, J.V., Slater, J.F., Wise, S.A., Cachier, H., Cary, R., Chow, J.C., Watson, J., Druffel, E.R.M., Masiello, C.A., Eglinton, T.I., Pearson, A., Reddy, C.M., Gustafsson, Ö., Quinn, J.G., Hartmann, P.C., et al., 2002. A critical evaluation of interlaboratory data on total, elemental, and isotopic carbon in the carbonaceous particle reference material, NIST SRM 1649a. J. Res. Natl. Inst. Stand. Technol. 107, 279–298.
Dai, M., Zhu, B., Fang, C., Zhou, S., Lu, W., Zhao, D., Ding, D., Pan, C., Liao, H., 2021. Long-term variation and source apportionment of black carbon at MT. Waliguan, China. J. Geophys. Res. Atmos. 126 e2021JD035273.
Dai, R., Zhu, Y., Zheng, S., Wang, J., Shan, M., Zhang, H., Chen, Y., Chen, R., Ma, J., Zhong, Q., Shen, H., Shen, G., Wang, C., Tao, S., 2025. Highly resolved global emissions and potential toxicities of 30 parent PAHs from 1960 to 2021. Environ. Sci. Technol. 59, 11677–11685.
Dai, T., Dai, Q., Ding, J., Liu, B., Bi, X., Wu, J., Zhang, Y., Feng, Y., 2023. Measuring the emission changes and meteorological dependence of source-specific BC aerosol using factor analysis coupled with machine learning. J. Geophys. Res. Atmos. 128 e2023JD038696.
Daly, H.M., Horn, A.B., 2009. Heterogeneous chemistry of toluene, kerosene and diesel soots. Phys. Chem. Chem. Phys. 11, 1069–1076.
Dao, X., Lin, Y., Cao, F., Di, S., Hong, Y., Xing, G., Li, J., Fu, P., Zhang, Y., 2019. Introduction to the national aerosol chemical composition monitoring network of China: objectives, current status, and outlook. Bull. Am. Meteorol. Soc. 100, ES337–ES351.
Deng, Y., Ikeda, K., Tanimoto, H., Andrews, E., Chan, T., Krejci, R., Heslin-Rees, D., Backman, J., Hyvärinen, A., Sharma, S., 2026. China's contribution to arctic black carbon declined from 2009 to 2022. Earths Future 14 e2025EF007441.
Dhada, I., Waziri, S.A. Vishal, Singha, S., Padhi, B.K., Samal, S.K., 2025. Expected health risk out of black carbon and particulate matter in the indoor environment of an industrial cluster of chandigarh in India. Sci. Rep. 15, 23177.
Ding, A., Huang, X., Nie, W., Sun, J., Kerminen, V.M., Petäjä, T., Su, H., Cheng, Y., Yang, X., Wang, M., Chi, X., Wang, J., Virkkula, A., Guo, W., Yuan, J., Wang, S., Zhang, R., Wu, Y., Song, Y., Zhu, T., et al., 2016. Enhanced haze pollution by black carbon in megacities in China. Geophys. Res. Lett. 43, 2873–2879.
Ding, Q., Sun, J., Huang, X., Ding, A., Zou, J., Yang, X., Fu, C., 2019a. Impacts of black carbon on the formation of advection-radiation fog during a haze pollution episode in eastern China. Atmos. Chem. Phys. 19, 7759–7774.
Ding, S., Liu, D., Zhao, D., Hu, K., Tian, P., Zhou, W., Huang, M., Yang, Y., Wang, F., Sheng, J., Liu, Q., Kong, S., Cui, P., Huang, Y., He, H., Coe, H., Ding, D., 2019b. Size-related physical properties of black carbon in the lower atmosphere over Beijing and Europe. Environ. Sci. Technol. 53, 11112–11121.
Ding, S., Zhao, D., He, C., Huang, M., He, H., Tian, P., Liu, Q., Bi, K., Yu, C., Pitt, J., Chen, N., Ma, X., Chen, Y., Jia, X., Kong, S., Wu, J., Hu, D., Hu, K., Ding, D., Liu, D., 2019c. Observed interactions between black carbon and hydrometeor during wet scavenging in mixed-phase clouds. Geophys. Res. Lett. 46, 8453–8463.
Dong, Z., Ma, J., Qiu, J., Ren, Q., Shan, Q., Duan, X., Li, G., Zuo, Y., Qi, Y., Liu, Y., 2023. Airborne fine particles drive H1N1 viruses deep into the lower respiratory tract and distant organs. Sci. Adv. 9 eadf2165.
Du, H., Li, J., Chen, X., Curci, G., Yu, F., Sun, Y., Dao, X., Guo, S., Wang, Z., Yang, W., Wei, L., Wang, Z., 2025. Modeling simulation of aerosol light absorption over the Beijing-Tianjin-Hebei region: the impact of mixing state and aging processes. Atmos. Chem. Phys. 25, 5665–5681.
Dunker, A.M., Morris, R.E., Pollack, A.K., Schleyer, C.H., Yarwood, G., 1996. Photochemical modeling of the impact of fuels and vehicles on urban ozone using auto/oil program data. Environ. Sci. Technol. 30, 787–801.
ECCC, 2025. Air pollutant emissions inventory. Environment and Climate Change Canada. Available at: https://www.canada.ca/en/environment-climate-change/services/pollutants/air-emissions-inventory-overview.html.
Elmquist, M., Cornelissen, G., Kukulska, Z., Gustafsson, Ö., 2006. Distinct oxidative stabilities of char versus soot black carbon: implications for quantification and environmental recalcitrance. Glob. Biogeochem. Cycles 20. GB2009.
Fang, C., Zhu, B., Pan, C., Yun, X., Ding, D., Tao, S., 2020. Regional and sectoral sources for black carbon over South China in spring and their sensitivity to East Asian summer monsoon onset. J. Geophys. Res. Atmos. 125 e2020JD033219.
Fang, Y., Chen, Y., Tian, C., Lin, T., Hu, L., Li, J., Zhang, G., 2016. Application of PMF receptor model merging with pahs signatures for source apportionment of black carbon in the continental shelf surface sediments of the Bohai and Yellow Seas, China. J. Geophys. Res. Oceans 121, 1346–1359.
Favez, O., El Haddad, I., Piot, C., Boréave, A., Abidi, E., Marchand, N., Jaffrezo, J.L., Besombes, J.L., Personnaz, M.B., Sciare, J., Wortham, H., George, C., D'Anna, B., 2010. Inter-comparison of source apportionment models for the estimation of wood burning aerosols during wintertime in an Alpine city (Grenoble, France). Atmos. Chem. Phys. 10, 5295–5314.
Fierce, L., Bond, T.C., Bauer, S.E., Mena, F., Riemer, N., 2016. Black carbon absorption at the global scale is affected by particle-scale diversity in composition. Nat. Commun. 7, 12361.
Fierce, L., Onasch, T.B., Cappa, C.D., Mazzoleni, C., China, S., Bhandari, J., Davidovits, P., Fischer, D.A., Helgestad, T., Lambe, A.T., Sedlacek 3rd, A.J., Smith, G.D., Wolff, L., 2020. Radiative absorption enhancements by black carbon controlled by particle-to-particle heterogeneity in composition. Proc. Natl. Acad. Sci. USA 117, 5196–5203.
Fu, B., Bellis, G.A., Hong, J., Wang, J., Wu, Q., Tang, Q., Cheng, J., Zhu, Z., 2012. Morphology, distribution, and abundance of antennal sensilla of male and female macropterous and brachypterous small brown planthopper, Laodelphax striatellus (Fallen) (Hemiptera: Delphacidae). Microsc. Res. Tech. 75, 1492–1512.
Gan, W., FitzGerald, J.M., Carlsten, C., Sadatsafavi, M., Brauer, M., 2013. Associations of ambient air pollution with chronic obstructive pulmonary disease hospitalization and mortality. Am. J. Respir. Crit. Care Med. 187, 721–727.
Geng, F., Hua, J., Mu, Z., Peng, L., Xu, X., Chen, R., Kan, H., 2013. Differentiating the associations of black carbon and fine particle with daily mortality in a Chinese city. Environ. Res. 120, 27–32.
Geng, X., Haig, J., Lin, B., Tian, C., Zhu, S., Cheng, Z., Yuan, Y., Zhang, Y., Liu, J., Zheng, M., Li, J., Zhong, G., Zhao, S., Bird, M.I., Zhang, G., 2023. Provenance of aerosol black carbon over northeast Indian ocean and South China sea and implications for oceanic black carbon cycling. Environ. Sci. Technol. 57, 13067–13078.
Goldberg, E.D., 1985. Black Carbon in the Environment: Properties and Distribution. John Wiley and Sons, New York.
Gong, X., Zhang, C., Chen, H., Nizkorodov, S.A., Chen, J., Yang, X., 2016. Size distribution and mixing state of black carbon particles during a heavy air pollution episode in Shanghai. Atmos. Chem. Phys. 16, 5399–5411.
Guan, C., Li, X., Zhang, W., Huang, Z., 2017. Identification of nitration products during heterogeneous reaction of $NO_2$ on soot in the dark and under simulated sunlight. J. Phys. Chem. A 121, 482–492.
Guan, X., Zhang, N., Tian, P., Tang, C., Zhang, Z., Wang, L., Zhang, Y., Zhang, M., Guo, Y., Du, T., Cao, X., Liang, J., Zhang, L., 2022. Wintertime vertical distribution of black carbon and single scattering albedo in a semi-arid region derived from tethered balloon observations. Sci. Total Environ. 807, 150790.
Guizzardi, D., Crippa, M., Butler, T., Keating, T., Wu, R., Kaminski, J., Kuenen, J., Kurokawa, J., Chatani, S., Morikawa, T., Pouliot, G., Racine, J., Moran, M.D.,

Klimont, Z., Manseau, P.M., Mashayekhi, R., Henderson, B.H., Smith, S.J., Hoesly, R., Muntean, M., et al., 2025. The HTAP_v3.2 emission mosaic: merging regional and global monthly emissions (2000-2020) to support air quality modelling and policies. Earth Syst. Sci. Data 17, 5915–5950.
Guo, B., Wang, Y., Zhang, X., Che, H., Ming, J., Yi, Z., 2020. Long-term variation of black carbon aerosol in China based on revised aethalometer monitoring data. Atmosphere 11, 684.
Guo, Q., Zhao, Y., Xue, T., Zhang, J., Duan, X., 2022. Association of $PM_{2.5}$ and its chemical compositions with metabolic syndrome: a nationwide study in middle-aged and older Chinese adults. Int. J. Environ. Res. Publ. Health 19, 14671.
Gustafsson, Ö., Bucheli, T.D., Kukulska, Z., Andersson, M., Largeau, C., Rouzaud, J.N., Reddy, C.M., Eglinton, T.I., 2001. Evaluation of a protocol for the quantification of black carbon in sediments. Glob. Biogeochem. Cycles 15, 881–890.
Gustafsson, Ö., Budhavant, K., Chimurkar, N., Clarke, S., Dreyfus, G., Gong, X., Klimont, Z., Klingmüller, K., Kim, S.W., Lelieveld, J., Myhre, G., Nair, H.R.C.R., Peng, J., Ramanathan, V., Rana, A., Manoj, M.R., Satheesh, S.K., Venkataraman, C., Zhang, Q., 2026. Atmospheric black carbon in the climate system. Nat. Rev. Earth Environ. 1–17.
Gustafsson, Ö., Kruså, M., Zencak, Z., Sheesley, R.J., Granat, L., Engström, E., Praveen, P. S., Rao, P.S.P., Leck, C., Rodhe, H., 2009. Brown clouds over South Asia: biomass or fossil fuel combustion? Science 323, 495–498.
Hakkarainen, H., Salo, L., Mikkonen, S., Saarikoski, S., Aurela, M., Teinilä, K., Ihalainen, M., Martikainen, S., Marjanen, P., Lepistö, T., Kuittinen, N., Saarnio, K., Aakko-Saksa, P., Pfeiffer, T.V., Timonen, H., Rönkkö, T., Jalava, P.I., 2022. Black carbon toxicity dependence on particle coating: measurements with a novel cell exposure method. Sci. Total Environ. 838, 156543.
Han, C., Liu, Y., He, H., 2013a. Heterogeneous photochemical aging of soot by $NO_2$ under simulated sunlight. Atmos. Environ. 64, 270–276.
Han, C., Liu, Y., He, H., 2013b. Role of organic carbon in heterogeneous reaction of $NO_2$ with soot. Environ. Sci. Technol. 47, 3174–3181.
Han, C., Liu, Y., He, H., 2016. The photoenhanced aging process of soot by the heterogeneous ozonization reaction. Phys. Chem. Chem. Phys. 18, 24401–24407.
Han, C., Liu, Y., Ma, J., He, H., 2012. Key role of organic carbon in the sunlight-enhanced atmospheric aging of soot by $O_2$. Proc. Natl. Acad. Sci. USA 109, 21250–21255.
Han, X., Cao, M., Pan, Z., Guo, J., Huang, D., Sun, W., Mi, J., Li, P., Liu, Y., Xue, T., Guan, T., 2023. Association between long-term exposure to $PM_{2.5}$ constituents and electrocardiographic abnormality: a nationwide longitudinal study in China. Environ. Int. 178, 108130.
Han, Y., Cai, J., Chen, Y., Zhang, Y., Jin, L., Chen, T., Li, J., Zhang, G., Chen, J., 2025. Concurrent formation of low-maturity EC and BrC in biomass and coal burning: O-PAH as a precursor. Environ. Sci. Technol. 59, 12083–12095.
Han, Y., Chen, Y., Feng, Y., Shang, Y., Li, J., Li, Q., Chen, J., 2021. Fuel aromaticity promotes low-temperature nucleation processes of elemental carbon from biomass and coal combustion. Environ. Sci. Technol. 55, 2532–2540.
Han, Y., Chen, Y., Feng, Y., Shang, Y., Li, J., Li, Q., Chen, J., 2022. Existence and formation pathways of high-and low-maturity elemental carbon from solid fuel combustion by a time-resolved study. Environ. Sci. Technol. 56, 2551–2561.
Han, Y., Lee, S., Cao, J., Ho, K., An, Z., 2009. Spatial distribution and seasonal variation of char-EC and soot-EC in the atmosphere over China. Atmos. Environ. 43, 6066–6073.
He, C., Li, Q., Liou, K.N., Qi, L., Tao, S., Schwarz, J.P., 2016. Microphysics-based black carbon aging in a global CTM: constraints from HIPPO observations and implications for global black carbon budget. Atmos. Chem. Phys. 16, 3077–3098.
He, C., Liou, K.N., Takano, Y., Zhang, R., Levy Zamora, M., Yang, P., Li, Q., Leung, L.R., 2015. Variation of the radiative properties during black carbon aging: theoretical and experimental intercomparison. Atmos. Chem. Phys. 15, 11967–11980.
He, G., He, H., 2020. Water promotes the oxidation of $SO_2$ by $O_2$ over carbonaceous aerosols. Environ. Sci. Technol. 54, 7070–7077.
He, G., Ma, J., He, H., 2018. Role of carbonaceous aerosols in catalyzing sulfate formation. ACS Catal. 8, 3825–3832.
Heringa, M.F., DeCarlo, P.F., Chirico, R., Lauber, A., Doberer, A., Good, J., Nussbaumer, T., Keller, A., Burtscher, H., Richard, A., Miljevic, B., Prevot, A.S.H., Baltensperger, U., 2012. Time-resolved characterization of primary emissions from residential wood combustion appliances. Environ. Sci. Technol. 46, 11418–11425.
Heringa, M.F., DeCarlo, P.F., Chirico, R., Tritscher, T., Dommen, J., Weingartner, E., Richter, R., Wehrle, G., Prévôt, A.S.H., Baltensperger, U., 2011. Investigations of primary and secondary particulate matter of different wood combustion appliances with a high-resolution time-of-flight aerosol mass spectrometer. Atmos. Chem. Phys. 11, 5945–5957.
Hoesly, R.M., Smith, S.J., Ahsan, H., Prime, N., O'Rourke, P., Crippa, M., Klimont, Z., Guizzardi, D., Feng, L., Harkins, C., Mcdonald, B., Wang, S., 2025. CEDS v_2025_04_18 Gridded Emissions Data 0.5 Degree (V_2025_03_18).
Hoesly, R.M., Smith, S.J., Feng, L., Klimont, Z., Janssens-Maenhout, G., Pitkanen, T., Seibert, J.J., Vu, L., Andres, R.J., Bolt, R.M., Bond, T.C., Dawidowski, L., Kholod, N., Kurokawa, J.I., Li, M., Liu, L., Lu, Z., Moura, M.C.P., O'Rourke, P.R., Zhang, Q., 2018. Historical (1750-2014) anthropogenic emissions of reactive gases and aerosols from the Community Emissions Data System (CEDS). Geosci. Model Dev. 11, 369–408.
Hou, W., Liu, Z., Yu, G., Bie, S., Zhang, Y., Chen, Y., Ma, D., Zhang, F., Lou, C., Hu, X., Gui, Y., Zhou, W., 2023. On-board measurements of OC/EC ratio, mixing state, and light absorption of ship-emitted particles. Sci. Total Environ. 904, 166692.
Hu, J., Yang, L., Kang, N., Wang, N., Shen, L., Zhang, X., Liu, S., Li, H., Xue, T., Ma, S., Zhu, T., 2025a. Associations between long-term exposure to fine particulate matter and its constituents with lung cancer incidence: evidence from a prospective cohort study in Beijing, China. Environ. Pollut. 368, 125686.
Hu, K., Zhao, D., Liu, D., Ding, S., Tian, P., Yu, C., Zhou, W., Huang, M., Ding, D., 2020. Estimating radiative impacts of black carbon associated with mixing state in the lower atmosphere over the northern North China Plain. Chemosphere 252, 126455.
Hu, S., Zeng, L., Zhao, G., Chen, S., Zhao, C., Zhao, W., Hu, M., 2025b. Significant changes in the physicochemical properties of BC-containing particles during the cold season in Beijing. J. Environ. Sci. 151, 667–676.
Hua, J., Yin, Y., Peng, L., Du, L., Geng, F., Zhu, L., 2014. Acute effects of black carbon and $PM_{2.5}$ on children asthma admissions: a time-series study in a chinese city. Sci. Total Environ. 481, 433–438.
Huang, J., Zhang, Z., Tao, J., Zhang, L., Nie, F., Fei, L., 2022. Source apportionment of carbonaceous aerosols using hourly data and implications for reducing $PM_{2.5}$ in the Pearl River Delta region of South China. Environ. Res. 210, 112960.
Huang, W., Baumgartner, J., Zhang, Y., Wang, Y., Schauer, J.J., 2015. Source apportionment of air pollution exposures of rural Chinese women cooking with biomass fuels. Atmos. Environ. 104, 79–87.
Huang, X., Peng, Y., Wei, J., Peng, J., Lin, X., Tang, M., Cheng, Y., Men, Z., Fang, T., Zhang, J., He, L., Cao, L., Liu, C., Zhang, C., Mao, H., Seinfeld, J.H., Wang, Y., 2024. Microphysical complexity of black carbon particles restricts their warming potential. One Earth 7, 136–145.
Huang, X., Wang, Z., Ding, A., 2018. Impact of aerosol-PBL interaction on haze pollution: multiyear observational evidences in North China. Geophys. Res. Lett. 45, 8596–8603.
Hughes, M., Kodros, J., Pierce, J., West, M., Riemer, N., 2018. Machine learning to predict the global distribution of aerosol mixing state metrics. Atmosphere 9, 15.
Huntzicker, J.J., Johnson, R., Shah, J., Cary, R., 1982. Analysis of organic and elemental carbon in ambient aerosols by a thermal-optical method. Part. Carbon: Atmos. Life Cycle 79–88.
Islam, M.M., Wathore, R., Zerriffi, H., Marshall, J.D., Bailis, R., Grieshop, A.P., 2021. In-use emissions from biomass and LPG stoves measured during a large, multi-year cookstove intervention study in rural India. Sci. Total Environ. 758, 143698.
Jacobson, M.Z., 2001. Strong radiative heating due to the mixing state of black carbon in atmospheric aerosols. Nature 409, 3.
Jacobson, M.Z., 2004. Climate response of fossil fuel and biofuel soot, accounting for soot's feedback to snow and sea ice albedo and emissivity. J. Geophys. Res. Atmos. 109, 15.
Janssen, N.A., Hoek, G., Simic-Lawson, M., Fischer, P., van Bree, L., ten Brink, H., Keuken, M., Atkinson, R.W., Anderson, H.R., Brunekreef, B., Cassee, F.R., 2011. Black carbon as an additional indicator of the adverse health effects of airborne particles compared with $PM_{10}$ and $PM_{2.5}$. Environ. Health Perspect. 119, 1691–1699.
Jiang, F., Liu, J., Huang, Z., Zheng, J., Zhang, G., 2020. Progress of the stable carbon and radiocarbon isotopes of black carbon aerosol. Chin. Sci. Bull. 65, 4095–4106.
Jiang, H., Liu, Y., Xie, Y., Liu, J., Chen, T., Ma, Q., He, H., 2019. Oxidation potential reduction of carbon nanomaterials during atmospheric-relevant aging: role of surface coating. Environ. Sci. Technol. 53, 10454–10461.
Jiang, S., Chen, L., Shen, J., Zhang, D., Wu, H., Wang, R., Zhang, S., Jiang, N., Li, W., 2023. Adverse effects of prenatal exposure to oxidized black carbon particles on the reproductive system of male mice. Toxics 11, 556.
Jiang, S., Shang, M., Mu, K., Jiang, N., Wen, H., Wang, R., Wu, H., Li, W., 2018. In vitro and in vivo toxic effects and inflammatory responses induced by carboxylated black carbon-lead complex exposure. Ecotoxicol. Environ. Saf. 165, 484–494.
Jiang, X., Han, Y., Qiu, X., Chai, Q., Zhang, H., Chen, X., Cheng, Z., Wang, Y., Fan, Y., Xue, T., Li, W., Gong, J., Zhu, T., 2021. Organic components of personal $PM_{2.5}$ exposure associated with inflammation: evidence from an untargeted exposomic approach. Environ. Sci. Technol. 55, 10589–10596.
Jiang, Y., Du, C., Chen, R., Hu, J., Zhu, X., Xue, X., He, Q., Lu, J., Ge, J., Huo, Y., Kan, H., 2024. Differential effects of fine particulate matter constituents on acute coronary syndrome onset. Nat. Commun. 15, 10848.
Kang, Z., Ma, P., Quan, J., Jia, X., Liao, Z., Cheng, Z., Wang, Q., Dai, L., Zhao, X., Zhang, Z., Yuan, T., Pan, Y., 2023. Observational evidence of the regional transported black carbon in high layer over Beijing. Atmos. Environ. 311, 120000.
Karavalakis, G., Gysel, N., Schmitz, D.A., Cho, A.K., Sioutas, C., Schauer, J.J., Cocker, D. R., Durbin, T.D., 2017. Impact of biodiesel on regulated and unregulated emissions, and redox and proinflammatory properties of PM emitted from heavy-duty vehicles. Sci. Total Environ. 584, 1230–1238.
Khalizov, A.F., Cruz-Quinones, M., Zhang, R., 2010. Heterogeneous reaction of $NO_2$ on fresh and coated soot surfaces. J. Phys. Chem. A 114, 7516–7524.
Kim, G., Jeon, S., Park, B., Jo, S.G., Moon, H.G., Kim, S.H., Huh, Y.S., Lee, K., Duffin, R., Cho, W.S., 2025. Lung-associated lymph nodes and spleen are major secondary accumulating organs in mice following inhaled black carbon as a surrogate of ultrafine ambient particles. Environ. Int. 199, 109475.
Kim, K.H., Jahan, S.A., Kabir, E., Brown, R.J.C., 2013. A review of airborne polycyclic aromatic hydrocarbons (PAHs) and their human health effects. Environ. Int. 60, 71–80.
Kleinman, M.T., Bufalino, C., Rasmussen, R., Hyde, D., Bhalla, D.K., Mautz, W.J., 2000. Toxicity of chemical components of ambient fine particulate matter ($PM_{2.5}$) inhaled by aged rats. J. Appl. Toxicol. 20, 357–364.
Kong, L., Tang, X., Zhu, J., Wang, Z., Liu, B., Zhu, Y., Zhu, L., Chen, D., Hu, K., Wu, H., Wu, Q., Shen, J., Sun, Y., Liu, Z., Xin, J., Ji, D., Zheng, M., 2024. High-resolution simulation dataset of hourly $PM_{2.5}$ chemical composition in China (CAQRA-aerosol) from 2013 to 2020. Adv. Atmos. Sci. 41, 1–16.
Kuang, Y., Guo, Y., Chai, J., Shang, J., Zhu, J., Stevanovic, S., Ristovski, Z., 2020. Comparison of light absorption and oxidative potential of biodiesel/diesel and chemicals/diesel blends soot particles. J. Environ. Sci. 87, 184–193.
Kurokawa, J., Ohara, T., 2020. Long-term historical trends in air pollutant emissions in Asia: regional Emission inventory in ASia (REAS) version 3. Atmos. Chem. Phys. 20, 12761–12793.

Lee, Y.H., Lamarque, J.F., Flanner, M.G., Jiao, C., Shindell, D.T., Berntsen, T., Bisiaux, M. M., Cao, J., Collins, W.J., Curran, M., Edwards, R., Faluvegi, G., Ghan, S., Horowitz, L.W., McConnell, J.R., Ming, J., Myhre, G., Nagashima, T., Naik, V., Rumbold, S.T., et al., 2013. Evaluation of preindustrial to present-day black carbon and its albedo forcing from Atmospheric Chemistry and climate model intercomparison project (ACCMIP). Atmos. Chem. Phys. 13, 2607–2634.
Leifeld, J., 2007. Thermal stability of black carbon characterised by oxidative differential scanning calorimetry. Org. Geochem. 38, 112–127.
Lelièvre, S., Bedjanian, Y., Laverdet, G., Le Bras, G., 2004. Heterogeneous reaction of $NO_2$ with hydrocarbon flame soot. J. Phys. Chem. A 108, 10807–10817.
Li, C., Borken-Kleefeld, J., Zheng, J., Yuan, Z., Ou, J., Li, Y., Wang, Y., Xu, Y., 2018a. Decadal evolution of ship emissions in China from 2004 to 2013 by using an integrated AIS-based approach and projection to 2040. Atmos. Chem. Phys. 18, 6075–6093.
Li, J., Wang, Y., Steenland, K., Liu, P., van Donkelaar, A., Martin, R.V., Chang, H., Caudle, W.M., Schwartz, J., Koutrakis, P., Shi, L., 2022a. Long-term effects of $PM_{2.5}$ components on incident dementia in the northeastern United States. Innovation 3, 100208.
Li, J., Zhang, Y., Zheng, S., Wang, J., Dai, R., Zhang, W., Xu, H., Shen, H., Shen, G., Cheng, H., Ma, J., Tao, S., 2024a. Mitigating black carbon emissions: key drivers in residential usage and coke/brick production. Natl. Sci. Rev. 11 nwae283.
Li, M., Bao, F., Zhang, Y., Song, W., Chen, C., Zhao, J., 2018b. Role of elemental carbon in the photochemical aging of soot. Proc. Natl. Acad. Sci. USA 115, 7717–7722.
Li, M., Dong, J., Huang, Z., Li, L., Gao, W., Nian, H., Fu, Z., Cheng, P., Zhou, Z., 2012. Analysis of cigarette smoke aerosol by single particle aerosol mass spectrometer. Chin. J. Anal. Chem. 40, 936–939.
Li, P., Xie, X., Wu, Y., Wang, J., Jin, Y., Guo, S., Hu, M., Hu, J., 2025a. Evolution of black carbon aging degree in China from 2013-2019 and key driving factors. Environ. Sci. Technol. Lett. 12, 1373–1379.
Li, Q., Shang, J., Zhu, T., 2013. Physicochemical characteristics and toxic effects of ozone-oxidized black carbon particles. Atmos. Environ. 81, 68–75.
Li, R., Han, Y., Wang, L., Shang, Y., Chen, Y., 2019. Differences in oxidative potential of black carbon from three combustion emission sources in China. J. Environ. Manag. 240, 57–65.
Li, S., Wang, S., Wu, Q., Zhang, Y., Ouyang, D., Zheng, H., Han, L., Qiu, X., Wen, Y., Liu, M., Jiang, Y., Yin, D., Liu, K., Zhao, B., Zhang, S., Wu, Y., Hao, J., 2023. Emission trends of air pollutants and $CO_2$ in China from 2005 to 2021. Earth Syst. Sci. Data 15, 2279–2294.
Li, W., Liu, X., Duan, F., Qu, Y., An, J., 2022b. A one-year study on black carbon in urban Beijing: concentrations, sources and implications on visibility. Atmos. Pollut. Res. 13, 101307.
Li, W., Riemer, N., Xu, L., Wang, Y., Adachi, K., Shi, Z., Zhang, D., Zheng, Z., Laskin, A., 2024b. Microphysical properties of atmospheric soot and organic particles: measurements, modeling, and impacts. npj Clim. Atmos. Sci. 7, 65.
Li, W., Shao, L., Zhang, D., Ro, C.U., Hu, M., Bi, X., Geng, H., Matsuki, A., Niu, H., Chen, J., 2016. A review of single aerosol particle studies in the atmosphere of East Asia: morphology, mixing state, source, and heterogeneous reactions. J. Clean. Prod. 112, 1330–1349.
Li, W., Wang, Y., Zeng, Z., Yi, Z., Che, H., Zhang, X., 2025b. Hourly estimation of black carbon in China based on sparse observation data and stacking model. Atmos. Environ. 350, 121164.
Liati, A., Spiteri, A., Eggenschwiler, P.D., Vogel-Schäuble, N., 2012. Microscopic investigation of soot and ash particulate matter derived from biofuel and diesel: implications for the reactivity of soot. J. Nano Res. 14, 1224.
Lin, C., Huang, R., Duan, J., Zhong, H., Xu, W., Wu, Y., Zhang, R., 2022. Large contribution from worship activities to the atmospheric soot particles in northwest China. Environ. Pollut. 299, 118907.
Lin, W., Huang, W., Zhu, T., Hu, M., Brunekreef, B., Zhang, Y., Liu, X., Cheng, H., Gehring, U., Li, C., Tang, X., 2011. Acute respiratory inflammation in children and black carbon in ambient air before and during the 2008 Beijing Olympics. Environ. Health Perspect. 119, 1507–1512.
Lippmann, M., Chen, L.C., 2009. Health effects of concentrated. Ambient air particulate matter (CAPs) and its components. Crit. Rev. Toxicol. 39, 865–913.
Liu, B., Wu, C., Ma, N., Chen, Q., Li, Y., Ye, J., Martin, S.T., Li, Y., 2020a. Vertical profiling of fine particulate matter and black carbon by using unmanned aerial vehicle in Macau. China. Sci. Total Environ. 709, 136109.
Liu, D., Joshi, R., Wang, J., Yu, C., Allan, J.D., Coe, H., Flynn, M.J., Xie, C., Lee, J., Squires, F., Kotthaus, S., Grimmond, S., Ge, X., Sun, Y., Fu, P., 2019a. Contrasting physical properties of black carbon in urban Beijing between winter and summer. Atmos. Chem. Phys. 19, 6749–6769.
Liu, D., Li, S., Hu, D., Kong, S., Cheng, Y., Wu, Y., Ding, S., Hu, K., Zheng, S., Yan, Q., 2021a. Evolution of aerosol optical properties from wood smoke in real atmosphere influenced by burning phase and solar radiation. Environ. Sci. Technol. 55, 5677–5688.
Liu, D., Whitehead, J., Alfarra, M.R., Reyes-Villegas, E., Spracklen, D.V., Reddington, C. L., Kong, S., Williams, P.I., Ting, Y., Haslett, S., Taylor, J.W., Flynn, M.J., Morgan, W. T., McFiggans, G., Coe, H., Allan, J.D., 2017. Black-carbon absorption enhancement in the atmosphere determined by particle mixing state. Nat. Geosci. 10, 184–188.
Liu, D., Zhao, D., Xie, Z., Yu, C., Chen, Y., Tian, P., Ding, S., Hu, K., Lowe, D., Liu, Q., 2019b. Enhanced heating rate of black carbon above the planetary boundary layer over megacities in summertime. Environ. Res. Lett. 14, 124003.
Liu, H., Lei, J., Liu, Y., Zhu, T., Chan, K., Chen, X., Wei, J., Deng, F., Li, G., Jiang, Y., Bai, L., Wang, K., Chen, J., Lan, Y., Xia, X., Wang, J., Wei, C., Li, Y., Chen, R., Gong, J., et al., 2025a. Hospital admissions attributable to reduced air pollution due to clean-air policies in China. Nat. Med. 31, 1688–1697.
Liu, H., Meng, Z., Lv, Z., Wang, X., Deng, F., Liu, Y., Zhang, Y., Shi, M., Zhang, Q., He, K., 2019c. Emissions and health impacts from global shipping embodied in US-China bilateral trade. Nat. Sustain. 2, 1027–1033.
Liu, H., Pan, X., Lei, S., Zhang, Y., Du, A., Tian, Y., Yao, W., Xin, J., Li, J., Sun, Y., Cao, J., Wang, Z., 2023a. Microphysical characteristics of black carbon from various emission sources. Atmos. Environ. 307, 119825.
Liu, H., Pan, X., Lei, S., Zhang, Y., Du, A., Yao, W., Tang, G., Wang, T., Xin, J., Li, J., Sun, Y., Cao, J., Wang, Z., 2023b. Vertical distribution of black carbon and its mixing state in the urban boundary layer in summer. Atmos. Chem. Phys. 23, 7225–7239.
Liu, H., Pan, X., Liu, D., Liu, X., Chen, X., Tian, Y., Sun, Y., Fu, P., Wang, Z., 2020b. Mixing characteristics of refractory black carbon aerosols at an urban site in Beijing. Atmos. Chem. Phys. 20, 5771–5785.
Liu, H., Wang, Q., Ye, J., Su, X., Zhang, T., Zhang, Y., Tian, J., Dong, Y., Chen, Y., Zhu, C., Han, Y., Cao, J., 2021b. Changes in source-specific black carbon aerosol and the induced radiative effects due to the COVID-19 lockdown. Geophys. Res. Lett. 48 e2021GL092987.
Liu, J., Fan, S., Horowitz, L.W., Levy, H., 2011. Evaluation of factors controlling long-range transport of black carbon to the Arctic. J. Geophys. Res. Atmos. 116, D04307.
Liu, J., Jiang, F., Wang, Q., Zhang, G., Li, J., Chen, W., Ding, P., Zhu, S., Cheng, Z., Zhang, X., Sha, Q., Huang, Z., Yuan, X., Zheng, J., Zhang, Y., Yan, C., Tian, C., Chen, Y., Yu, J., Gustafsson, Ö., 2025b. Substantial reductions in black carbon from both fossil fuels and biomass burning during China's clean air action. Proc. Natl. Acad. Sci. USA 122, e2500843122.
Liu, S., Aiken, A.C., Gorkowski, K., Dubey, M.K., Cappa, C.D., Williams, L.R., Herndon, S. C., Massoli, P., Fortner, E.C., Chhabra, P.S., Brooks, W.A., Onasch, T.B., Jayne, J.T., Worsnop, D.R., China, S., Sharma, N., Mazzoleni, C., Xu, L., Ng, N.L., Liu, D., et al., 2015. Enhanced light absorption by mixed source black and brown carbon particles in UK winter. Nat. Commun. 6, 8435.
Liu, S., Geng, G., Xiao, Q., Zheng, Y., Liu, X., Cheng, J., Zhang, Q., 2022a. Tracking daily concentrations of $PM_{2.5}$ chemical composition in China since 2000. Environ. Sci. Technol. 56, 16517–16527.
Liu, X., Zheng, M., Liu, Y., Jin, Y., Liu, J., Zhang, B., Yang, X., Wu, Y., Zhang, T., Xiang, Y., Liu, B., Yan, C., 2022b. Intercomparison of equivalent black carbon (eBC) and elemental carbon (EC) concentrations with three-year continuous measurement in Beijing, China. Environ. Res. 209, 112791.
Liu, Y., Liu, J., Yan, C., Xiao, J., Ye, J., Guo, L., Zheng, M., 2023c. Metrological traceability of black carbon measurement based on optical methods and its challenges in China: a review. Atmos. Res. 292, 106854.
Liu, Y., Wang, Y., Cao, Y., Yang, X., Zhang, T., Luan, M., Lyu, D., Hansen, A.D.A., Liu, B., Zheng, M., 2021c. Impacts of COVID-19 on black carbon in two representative regions in China: insights based on online measurement in Beijing and Tibet. Geophys. Res. Lett. 48.
Liu, Y., Wu, L., Huang, S., Song, Q., Hu, W., Chen, W., Wu, Z., Man, R., He, Y., Li, W., Peng, Y., Liu, J., Song, W., Ma, N., Yuan, B., Wang, X., Shao, M., 2023d. Sources, size-resolved deposition in the human respiratory tract and health risks of submicron black carbon in urban atmosphere in Pearl River Delta. China. Sci. Total Environ. 891, 164391.
Liu, Y., Yan, C., Zheng, M., 2018. Source apportionment of black carbon during winter in Beijing. Sci. Total Environ. 618, 531–541.
Ljungman, P.L.S., Andersson, N., Stockfelt, L., Andersson, E.M., Nilsson Sommar, J., Eneroth, K., Gidhagen, L., Johansson, C., Lager, A., Leander, K., Molnar, P., Pedersen, N.L., Rizzuto, D., Rosengren, A., Segersson, D., Wennberg, P., Barregard, L., Forsberg, B., Sallsten, G., Bellander, T., et al., 2019. Long-term exposure to particulate air pollution, black carbon, and their source components in relation to ischemic heart disease and stroke. Environ. Health Perspect. 127, 107012.
Longfellow, C.A., Ravishankara, A.R., Hanson, D.R., 1999. Reactive uptake on hydrocarbon soot: Focus on $NO_2$. J. Geophys. Res. Atmos. 104, 13833–13840.
Loukhovitskaya, E.E., Talukdar, R.K., Ravishankara, A.R., 2013. Uptake of $HNO_3$ on aviation kerosene and aircraft engine soot: influences of $H_2O$ or/and $H_2SO_4$. J. Phys. Chem. A 117, 4928–4936.
Lu, W., Zhu, B., Liu, X., Dai, M., Shi, S., Gao, J., Yan, S., 2023. The influence of regional transport on the three-dimensional distributions of black carbon and its sources over eastern China. Atmos. Environ. 297, 119585.
Luan, M., Zhang, T., Li, X., Yan, C., Sun, J., Zhi, G., Shen, G., Liu, X., Zheng, M., 2022. Investigating the relationship between mass concentration of particulate matter and reactive oxygen species based on residential coal combustion source tests. Environ. Res. 212, 113499.
Ma, J., Li, L., Zhang, Z., Pei, Z., Zuo, P., Li, H., Yang, R., Li, Y., Zhang, Q., 2023. Insight into the oxidation of glutathione mediated by black carbon from three typical emission sources. Environ. Pollut. 316, 120647.
Ma, Q., Ma, J., Chu, B., Liu, Y., Lai, C., He, H., 2015. Current progress towards the heterogeneous reactions on mineral dust and soot. Chin. Sci. Bull. 60, 122–136.
Mak, J., Gross, S., Bertram, A.K., 2007. Uptake of $NO_3$ on soot and pyrene surfaces. Geophys. Res. Lett. 34, L10804.
Masiello, C.A., 2004. New directions in black carbon organic geochemistry. Mar. Chem. 92, 201–213.
Masiello, C.A., Druffel, E.R.M., Currie, L.A., 2002. Radiocarbon measurements of black carbon in aerosols and ocean sediments. Geochem. Cosmochim. Acta 66, 1025–1036.
Matsui, H., 2016. Black carbon simulations using a size-and mixing-state-resolved three-dimensional model: 2. Aging timescale and its impact over East Asia. J J. Geophys. Res. Atmos. 121, 1808–1821.
Matsui, H., Koike, M., Kondo, Y., Moteki, N., Fast, J.D., Zaveri, R.A., 2013. Development and validation of a black carbon mixing state resolved three-dimensional model: aging processes and radiative impact. J. Geophys. Res. Atmos. 118, 2304–2326.

McWhinney, R.D., Badali, K., Liggio, J., Li, S., Abbatt, J.P.D., 2013. Filterable redox cycling activity: a comparison between diesel exhaust particles and secondary organic aerosol constituents. Environ. Sci. Technol. 47, 3362–3369.
Meng, Q., Zhang, Y., Zhong, S., Chen, C., Yang, Y., Ge, X., 2024. Quantifying urban black carbon absorption enhancement under influence of open crop straw burning in eastern China. Sustain. Horiz. 12, 100113.
Ministry of Ecology and Environment of the People's Republic of China, 2012. Ambient Air Quality Standards (GB 3095-2012). China Environmental Science Press, Beijing.
Misaki, K., Takano, H., Kanazawa, H., Inoue, K.I., 2021. Biological response-enhancing activity with antigens in a549 cells exposed to representative polycyclic aromatic hydrocarbons. ACS Omega 6, 22224–22232.
Monge, M.E., D'Anna, B., Mazri, L., Giroir-Fendler, A., Ammann, M., Donaldson, D.J., George, C., 2010. Light changes the atmospheric reactivity of soot. Proc. Natl. Acad. Sci. USA 107, 6605–6609.
Muñoz, M.S.S., Rossi, M.J., 2002. Heterogeneous reactions of $HNO_3$ with flame soot generated under different combustion conditions. Reaction mechanism and kinetics. Phys. Chem. Chem. Phys. 4, 5110–5118.
Niranjan, R., Thakur, A.K., 2017. The toxicological mechanisms of environmental soot (black carbon) and carbon black: focus on oxidative stress and inflammatory pathways. Front. Immunol. 8, 763.
Noble, C.A., Prather, K.A., 1996. Real-time measurement of correlated size and composition profiles of individual atmospheric aerosol particles. Environ. Sci. Technol. 30, 2667–2680.
Nordmann, S., Cheng, Y., Carmichael, G.R., Yu, M., Denier van der Gon, H.A.C., Zhang, Q., Saide, P.E., Pöschl, U., Su, H., Birmili, W., Wiedensohler, A., 2014. Atmospheric black carbon and warming effects influenced by the source and absorption enhancement in central Europe. Atmos. Chem. Phys. 14, 12683–12699.
Novakov, T., 1984. The role of soot and primary oxidants in atmospheric chemistry. Sci. Total Environ. 36, 1–10.
Nze-Dike, O.U., Ezealisiji, K.M., Ezejiofor, A.N., Awanye, A.M., Dike, C.S., 2025. Genotoxic and epigenetic concerns of black carbon/soot in recent times: a systematic review. Discov. Appl. Sci. 7, 1140.
Onasch, T.B., Trimborn, A., Fortner, E.C., Jayne, J.T., Kok, G.L., Williams, L.R., Davidovits, P., Worsnop, D.R., 2012. Soot particle aerosol mass spectrometer: development, validation, and initial application. Aerosol Sci. Technol. 46, 804–817.
Oshima, N., Koike, M., 2013. Development of a parameterization of black carbon aging for use in general circulation models. Geosci. Model Dev. 6, 263–282.
Oshima, N., Koike, M., Zhang, Y., Kondo, Y., 2009. Aging of black carbon in outflow from anthropogenic sources using a mixing state resolved model: 2. Aerosol optical properties and cloud condensation nuclei activities. J. Geophys. Res. Atmos. 114, D18202.
Pan, X., Zhang, Y., Xue, C., Kuhn, U., Hrabe de Angelis, I., Pöhlker, C., Ditas, J., Heins, L., Aardema, H.M., Slagter, H.A., Calleja, M.L., Dragoneas, A., Walter, D., Nillius, B., Wang, Q., Ma, N., Su, H., Pöschl, U., Haug, G.H., Schiebel, R., et al., 2026. Black carbon in the marine atmosphere: concentration and mixing state from coastal to remote atlantic regions. J. Geophys. Res. Atmos. 131 e2025JD045346.
Pang, Y., Wang, Y., Wang, Z., Zhang, Y., Liu, L., Kong, S., Liu, F., Shi, Z., Li, W., 2022. Quantifying the fractal dimension and morphology of individual atmospheric soot aggregates. J. Geophys. Res. Atmos. 127 e2021JD036055.
Peng, B., Dong, Q., Li, F., Wang, T., Qiu, X., Zhu, T., 2023a. A systematic review of polycyclic aromatic hydrocarbon derivatives: occurrences, levels, biotransformation, exposure biomarkers, and toxicity. Environ. Sci. Technol. 57, 15314–15335.
Peng, J., Hu, M., Guo, S., Du, Z., Zheng, J., Shang, D., Zamora, M., Zeng, L., Shao, M., Wu, Y., Zheng, J., Wang, Y., Glen, C.R., Collins, D.R., Molina, M.J., Zhang, R., 2016. Markedly enhanced absorption and direct radiative forcing of black carbon under polluted urban environments. Proc. Natl. Acad. Sci. USA 113, 4266–4271.
Peng, R.D., Bell, M.L., Geyh, A.S., McDermott, A., Zeger, S.L., Samet, J.M., Dominici, F., 2009. Emergency admissions for cardiovascular and respiratory diseases and the chemical composition of fine particle air pollution. Environ. Health Perspect. 117, 957–963.
Peng, Y., Cai, J., Feng, Y., Jiang, H., Chen, Y., 2023b. Emission characteristic of OVOCs, I/SVOCs, OC and EC from wood combustion at different moisture contents. Atmos. Environ. 298, 119620.
Petzold, A., Ogren, J.A., Fiebig, M., Laj, P., Li, S., Baltensperger, U., Holzer-Popp, T., Kinne, S., Pappalardo, G., Sugimoto, N., Wehrli, C., Wiedensohler, A., Zhang, X., 2013. Recommendations for reporting "black carbon" measurements. Atmos. Chem. Phys. 13, 8365–8379.
Qi, L., Li, Q., He, C., Wang, X., Huang, J., 2017. Effects of the wegener-bergeron-findeisen process on global black carbon distribution. Atmos. Chem. Phys. 17, 7459–7479.
Qi, L., Wang, S., 2019a. Fossil fuel combustion and biomass burning sources of global black carbon from GEOS-Chem simulation and carbon isotope measurements. Atmos. Chem. Phys. 19, 11545–11557.
Qi, L., Wang, S., 2019b. Sources of black carbon in the atmosphere and in snow in the Arctic. Sci. Total Environ. 691, 442–454.
Ray, D., Bhattacharya, T.S., Chatterjee, A., Singha, A., Ghosh, S.K., Raha, S., 2018. Hygroscopic coating of sulfuric acid shields oxidant attack on the atmospheric pollutant benzo(a) pyrene bound to model soot particles. Sci. Rep. 8, 129.
Riemer, N., West, M., Zaveri, R., Easter, R., 2010. Estimating black carbon aging time-scales with a particle-resolved aerosol model. J. Aerosol Sci. 41, 143–158.
Rönkkö, T., Saarikoski, S., Kuittinen, N., Karjalainen, P., Keskinen, H., Järvinen, A., Mylläri, F., Aakko-Saksa, P., Timonen, H., 2023. Review of black carbon emission factors from different anthropogenic sources. Environ. Res. Lett. 18, 033004.
Roy, D., Lim, H., Kim, S., Song, S., Park, J., 2024. Particulate matter and black carbon exposure in seoul subway: implications for human health risk. J. Build. Eng. 95, 110091.
Sand, M., Samset, B.H., Myhre, G., Gliß, J., Bauer, S.E., Bian, H., Chin, M., Checa-Garcia, R., Ginoux, P., Kipling, Z., Kirkevåg, A., Kokkola, H., Le Sager, P., Lund, M.T., Matsui, H., van Noije, T., Olivié, D.J.L., Remy, S., Schulz, M., Stier, P., et al., 2021. Aerosol absorption in global models from AeroCom phase III. Atmos. Chem. Phys. 21, 15929–15947.
Sandradewi, J., Prévôt, A.S., Szidat, S., Perron, N., Alfarra, M.R., Lanz, V.A., Weingartner, E., Baltensperger, U., 2008a. Using aerosol light absorption measurements for the quantitative determination of wood burning and traffic emission contributions to particulate matter. Environ. Sci. Technol. 42, 3316.
Sandradewi, J., Prévôt, A.S.H., Weingartner, E., Schmidhauser, R., Gysel, M., Baltensperger, U., 2008b. A study of wood burning and traffic aerosols in an Alpine valley using a multi-wavelength aethalometer. Atmos. Environ. 42, 101–112.
Sedlacek, A.J., Lewis, E.R., Kleinman, L., Xu, J., Zhang, Q., 2012. Determination of and evidence for non-core-shell structure of particles containing black carbon using the Single-Particle Soot Photometer (SP2). Geophys. Res. Lett. 39, L06802.
Sha, Q., Zhu, M., Huang, H., Wang, Y., Huang, Z., Zhang, X., Tang, M., Lu, M., Chen, C., Shi, B., Chen, Z., Wu, L., Zhong, Z., Li, C., Xu, Y., Yu, F., Jia, G., Liao, S., Cui, X., Liu, J., et al., 2021. A newly integrated dataset of volatile organic compounds (VOCs) source profiles and implications for the future development of VOCs profiles in China. Sci. Total Environ. 793, 148348.
Shan, M., Dai, R., Zhu, Y., Zheng, S., Wang, J., Zhang, H., Chen, Y., Chen, R., Ma, J., Shen, G., Cheng, H., Zhong, Q., Shen, H., Wang, C., Tao, S., 2025. Trends in global black carbon emissions and population exposure from 1700 to 2021. Environ. Sci. Technol. 59, 12211–12220.
Shang, Y., Zhao, K., Xue, W., An, J., Zhong, Y., Chen, Y., Zeng, Q., Tang, Q., Qiu, X., 2024. Comparative assessment of acute neurotoxicity of real-world ultra-fine black carbon emitted from residential solid fuel combustion. Sci. Total Environ. 954, 176597.
Shen, G., Tao, S., Wei, S., Zhang, Y., Wang, R., Wang, B., Li, W., Shen, H., Huang, Y., Chen, Y., Chen, H., Yang, Y., Wang, W., Wei, W., Wang, X., Liu, W., Wang, X., Simonich, S.L.M., 2012. Reductions in emissions of carbonaceous particulate matter and polycyclic aromatic hydrocarbons from combustion of biomass pellets in comparison with raw fuel burning. Environ. Sci. Technol. 46, 6409–6416.
Shen, G., Yang, Y., Wang, W., Tao, S., Zhu, C., Min, Y., Xue, M., Ding, J., Wang, B., Wang, R., Shen, H., Li, W., Wang, X., Russell, A.G., 2010. Emission factors of particulate matter and elemental carbon for crop residues and coals burned in typical household stoves in China. Environ. Sci. Technol. 44, 7157–7162.
Shen, H., Huang, Y., Wang, R., Zhu, D., Li, W., Shen, G., Wang, B., Zhang, Y., Chen, Y., Lu, Y., Chen, H., Li, T., Sun, K., Li, B., Liu, W., Liu, J., Tao, S., 2013. Global atmospheric emissions of polycyclic aromatic hydrocarbons from 1960 to 2008 and future predictions. Environ. Sci. Technol. 47, 6415–6424.
Shen, W., Wang, M., Dong, X., 2024a. Enhanced aging of black carbon under recent clean air actions and future carbon neutrality scenario in China. Environ. Sci. Technol. 58, 13697–13706.
Shen, W., Wang, M., Riemer, N., Zheng, Z., Liu, Y., Dong, X., 2024b. Improving BC mixing state and CCN activity representation with machine learning in the Community Atmosphere Model Version 6 (CAM6). J. Adv. Model. Earth Syst. 16 e2023MS003889.
Shen, W., Wang, M., Wang, J., Liu, Y., Dong, X., Shao, X., Yue, M., Liu, Y., 2026. Quantifying global black carbon aging responses to emission reductions using a machine learning-based climate model. Adv. Atmos. Sci. 43, 361–372.
Shrestha, G., Traina, S.J., Swanston, C.W., 2010. Black carbon's properties and role in the environment: a comprehensive review. Sustainability 2, 294–320.
Smith, K.R., Jerrett, M., Anderson, H.R., Burnett, R.T., Stone, V., Derwent, R., Atkinson, R.W., Cohen, A., Shonkoff, S.B., Krewski, D., Pope, C.A., Thun, M.J., Thurston, G., 2009. Public health benefits of strategies to reduce greenhouse-gas emissions: health implications of short-lived greenhouse pollutants. Lancet 374, 2091–2103.
Song, W., He, K., Lei, Y., 2012. Black carbon emissions from on-road vehicles in China, 1990-2030. Atmos. Environ. 51, 320–328.
Sun, J., Xie, C., Xu, W., Chen, C., Ma, N., Xu, W., Lei, L., Li, Z., He, Y., Qiu, Y., Wang, Q., Pan, X., Su, H., Cheng, Y., Wu, C., Fu, P., Wang, Z., Sun, Y., 2021. Light absorption of black carbon and brown carbon in winter in North China Plain: comparisons between urban and rural sites. Sci. Total Environ. 770, 144821.
Sun, J., Zhi, G., Jin, W., Chen, Y., Shen, G., Tian, C., Zhang, Y., Zong, Z., Cheng, M., Zhang, X., Zhang, Y., Liu, C., Lu, J., Wang, H., Xiang, J., Tong, L., Zhang, X., 2018. Emission factors of organic carbon and elemental carbon for residential coal and biomass fuels in China- a new database for 39 fuel-stove combinations. Atmos. Environ. 190, 241–248.
Sun, T., Wu, C., Wu, D., Liu, B., Sun, J., Mao, X., Yang, H., Deng, T., Song, L., Li, M., Li, Y., Zhou, Z., 2020. Time-resolved black carbon aerosol vertical distribution measurements using a 356-m meteorological tower in Shenzhen. Theor. Appl. Climatol. 140, 1263–1276.
Szidat, S., Jenk, T.M., Synal, H.A., Kalberer, M., Wacker, L., Hajdas, I., Kasper-Giebl, A., Baltensperger, U., 2006. Contributions of fossil fuel, biomass-burning, and biogenic emissions to carbonaceous aerosols in Zurich as traced by $^{14}C$. J. Geophys. Res. Atmos. 111 (12), D07206.
Tan, T., Guo, S., Wu, Z., He, L., Huang, X., Hu, M., 2020. Impact of aging process on atmospheric black carbon aerosol properties and climate effects. Chin. Sci. Bull. 65, 4235–4250.
Tang, R., Cao, J., Shang, J., Kuang, Y., Geng, H., Qiu, X., 2024a. Coupling effect of elemental carbon and organic carbon on the changes of optical properties and oxidative potential of soot particles under visible light. Environ. Sci. Technol. 58, 19832–19842.

Tang, R., Shang, J., Qiu, X., Gong, J., Xue, T., Zhu, T., 2024b. Origin, structural characteristics, and health effects of atmospheric soot particles: a review. Curr. Pollut. Rep. 10, 532–547.
Tian, P., Liu, D., Zhao, D., Yu, C., Liu, Q., Huang, M., Deng, Z., Ran, L., Wu, Y., Ding, S., Hu, K., Zhao, G., Zhao, C., Ding, D., 2020. In situ vertical characteristics of optical properties and heating rates of aerosol over Beijing. Atmos. Chem. Phys. 20, 2603–2622.
Tian, Y., Ma, Y., Wu, J., Wu, Y., Wu, T., Hu, Y., Wei, J., 2024. Ambient $PM_{2.5}$ chemical composition and cardiovascular disease hospitalizations in China. Environ. Sci. Technol. 58, 16327–16335.
U.S. EPA, 2026. National Emissions Inventory (NEI). U.S. Environmental Protection Agency. Available at: https://www.epa.gov/air-emissions-inventories/national-emissions-inventory-nei.
Wang, H., Rasch, P.J., Easter, R.C., Singh, B., Zhang, R., Ma, P., Qian, Y., Ghan, S.J., Beagley, N., 2014a. Using an explicit emission tagging method in global modeling of source-receptor relationships for black carbon in the Arctic: variations, sources, and transport pathways. J. Geophys. Res. Atmos. 119, 12,888-812,909.
Wang, J., Jiang, H., Chen, Y., Han, Y., Cai, J., Peng, Y., Feng, Y., 2023a. Emission characteristics and influencing mechanisms of PAHs and EC from the combustion of three components (cellulose, hemicellulose, lignin) of biomasses. Sci. Total Environ. 859, 160359.
Wang, J., Wang, J., Cai, R., Liu, C., Jiang, J., Nie, W., Wang, J., Moteki, N., Zaveri, R.A., Huang, X., Ma, N., Chen, G., Wang, Z., Jin, Y., Cai, J., Zhang, Y., Chi, X., Holanda, B. A., Xing, J., Liu, T., et al., 2023b. Unified theoretical framework for black carbon mixing state allows greater accuracy of climate effect estimation. Nat. Commun. 14, 2703.
Wang, Q., Schwarz, J.P., Cao, J., Gao, R., Fahey, D.W., Hu, T., Huang, R.J., Han, Y., Shen, Z., 2014b. Black carbon aerosol characterization in a remote area of Qinghai-Tibetan Plateau, western China. Sci. Total Environ. 479, 151–158.
Wang, R., Tao, S., Wang, W., Liu, J., Shen, H., Shen, G., Wang, B., Liu, X., Li, W., Huang, Y., Zhang, Y., Lu, Y., Chen, H., Chen, Y., Wang, C., Zhu, D., Wang, X., Li, B., Liu, W., Ma, J., 2012. Black carbon emissions in China from 1949 to 2050. Environ. Sci. Technol. 46, 7595–7603.
Wang, Y., Li, W., Huang, J., Liu, L., Pang, Y., He, C., Liu, F., Liu, D., Bi, L., Zhang, X., Shi, Z., 2021a. Nonlinear enhancement of radiative absorption by black carbon in response to particle mixing structure. Geophys. Res. Lett. 48 e2021GL096437.
Wang, Y., Li, X., Shi, Z., Huang, L., Li, J., Zhang, H., Ying, Q., Wang, M., Ding, D., Zhang, X., Hu, J., 2021b. Premature mortality associated with exposure to outdoor black carbon and its source contributions in China. Resour. Conserv. Recycl. 170, 105620.
Wang, Y., Zheng, Z., Sun, Y., Yao, Y., Ma, P., Zhang, A., Zhu, S., Zhang, Z., Chen, X., Pang, Y., Wang, Q., Che, H., Ching, J., Li, W., 2025. Improved representation of black carbon mixing structures suggests stronger direct radiative heating. One Earth 8, 101311.
Wang, Z., Chien, C.J., Tonnesen, G.S., 2009. Development of a tagged species source apportionment algorithm to characterize three-dimensional transport and transformation of precursors and secondary pollutants. J. Geophys. Res. Atmos. 114, D21206.
Wei, C., Larson, S.M., Patten, K.O., Wuebbles, D.J., 2001. Modeling of ozone reactions on aircraft-related soot in the upper troposphere and lower stratosphere. Atmos. Environ. 35, 6167–6180.
Wei, J., Li, Z., Chen, X., Li, C., Sun, Y., Wang, J., Lyapustin, A., Brasseur, G.P., Jiang, M., Sun, L., Wang, T., Jung, C., Qiu, B., Fang, C., Liu, X., Hao, J., Wang, Y., Zhan, M., Song, X., Liu, Y., 2023a. Separating daily 1 km $PM_{2.5}$ inorganic chemical composition in China since 2000 via deep learning integrating ground, satellite, and model data. Environ. Sci. Technol. 57, 18282–18295.
Wei, J., Wang, J., Li, Z., Kondragunta, S., Anenberg, S., Wang, Y., Zhang, H., Diner, D., Hand, J., Lyapustin, A., Kahn, R., Colarco, P., da Silva, A., Ichoku, C., 2023b. Long-term mortality burden trends attributed to black carbon and $PM_{2.5}$ from wildfire emissions across the continental USA from 2000 to 2020: a deep learning modelling study. Lancet Planet. Health 7, 963–975.
Winiger, P., Andersson, A., Eckhardt, S., Stohl, A., Gustafsson, Ö., 2016. The sources of atmospheric black carbon at a European gateway to the Arctic. Nat. Commun. 7, 12776.
World Health Organization, 2021. World Health Statistics 2021: Monitoring Health for the Sdgs, Sustainable Development Goals. World Health Organization, Geneva.
Wu, Q., Zeng, H., Andersson, J., Oudin, A., Kanninen, K.M., Xu, M., Qin, S., Zeng, Q., Zhao, B., Zheng, M., Jin, N., Chou, W., Jalava, P., Dong, G., Zeng, X., 2024. Long-term exposure to major constituents of fine particulate matter and neurodegenerative diseases: a population-based survey in the Pearl River Delta region, China. J. Hazard. Mater. 470, 134161.
Wu, Y., Xia, Y., Zhou, C., Tian, P., Tao, J., Huang, R.J., Liu, D., Wang, X., Xia, X., Han, Z., Zhang, R., 2021. Effect of source variation on the size and mixing state of black carbon aerosol in urban Beijing from 2013 to 2019: implication on light absorption. Environ. Pollut. 270, 116089.
Xie, C., Xu, W., Wang, J., Liu, D., Ge, X., Zhang, Q., Wang, Q., Du, W., Zhao, J., Zhou, W., Li, J., Fu, P., Wang, Z., Worsnop, D., Sun, Y., 2019. Light absorption enhancement of black carbon in urban Beijing in summer. Atmos. Environ. 213, 499–504.
Xie, Y., Zeng, L., Hu, S., Wang, T., Du, Z., Tan, T., Xu, N., Chen, S., Mao, J., Xu, F., Hu, M., 2025. Long-term trends of black carbon levels, sources, and radiative effects from 2013 to 2022 in Beijing, China. npj Clean Air 1, 10.
Xiong, Q., Yu, H., Wang, R., Wei, J., Verma, V., 2017. Rethinking dithiothreitol-based particulate matter oxidative potential: measuring dithiothreitol consumption versus reactive oxygen species generation. Environ. Sci. Technol. 51, 6507–6514.
Xiong, R., Li, J., Zhang, Y., Zhang, L., Jiang, K., Zheng, H., Kong, S., Shen, H., Cheng, H., Shen, G., Tao, S., 2022. Global brown carbon emissions from combustion sources. Environ. Sci. Ecotechnol. 12, 100201.
Xu, H., Cai, J., Feng, X., Jiang, H., Peng, Y., Lu, Y., Chen, Y., 2025. Chemical and optical distinctions between elemental carbon subcategories Char-EC and Soot-EC: insights from a haze event in North China. Environ. Pollut. 375, 126306.
Xu, W., Li, Q., Shang, J., Liu, J., Feng, X., Zhu, T., 2015. Heterogeneous oxidation of $SO_2$ by $O_3$-aged black carbon and its dithiothreitol oxidative potential. J. Environ. Sci. 36, 56–62.
Xu, Y., Chen, X., Han, Y., Chen, W., Wang, T., Gong, J., Fan, Y., Zhang, H., Zhang, L., Li, H., Wang, Q., Yao, Y., Xue, T., Wang, J., Qiu, X., Que, C., Zheng, M., Zhu, T., 2022. Ceramide metabolism mediates the impaired glucose homeostasis following short-term black carbon exposure: a targeted lipidomic analysis. Sci. Total Environ. 829, 154657.
Xu, Y., Ramanathan, V., Washington, W.M., 2016. Observed high-altitude warming and snow cover retreat over Tibet and the himalayas enhanced by black carbon aerosols. Atmos. Chem. Phys. 16, 1303–1315.
Yang, J., Kang, S., Ji, Z., Chen, D., 2018. Modeling the origin of anthropogenic black carbon and its climatic effect over the Tibetan Plateau and surrounding regions. J. Geophys. Res. Atmos. 123, 671–692.
Yang, L., Kang, N., Wang, N., Zhang, X., Liu, S., Li, H., Cao, L., Xue, T., Li, Z., Ji, J., Zhu, T., 2024. Specifying the associations between $PM_{2.5}$ constituents and gastrointestinal cancer incidence: findings from a prospective cohort study in Beijing, China. Environ. Sci. Technol. 58, 21489–21498.
Yang, L., Zhang, Q., Lv, Z., Zhao, J., Zou, C., Wei, N., Jia, Z., Zhang, Y., Fu, F., Lv, J., Wu, L., Wang, T., Peng, J., Mao, H., 2023. Real world emission characteristics of chinese fleet and the current situation of underestimated ship emissions. J. Clean. Prod. 418, 138107.
Yang, X., Cao, F., Lin, Y., Fan, M., Wu, C., Yu, M., Song, W., Zhang, Y., 2025a. Distinct sources of char and soot black carbon aerosols during winter haze at pair sites in North China: source apportionment from dual-carbon isotope constrained PMF. J. Geophys. Res. Atmos. 130 e2024JD043077.
Yang, X., Shi, M., Gao, K., Wang, X., Zhou, L., Chen, J., 2025b. Environmentally persistent free radicals on black carbon induce rapid degradation of phenolic acids. Environ. Sci. Technol. 59, 17116–17125.
Yang, Y., Wang, H., Smith, S.J., Ma, P., Rasch, P.J., 2017. Source attribution of black carbon and its direct radiative forcing in China. Atmos. Chem. Phys. 17, 4319–4336.
Yi, W., Wang, X., He, T., Liu, H., Luo, Z., Lv, Z., He, K., 2025. The high-resolution global shipping emission inventory by the Shipping Emission Inventory Model (SEIM). Earth Syst. Sci. Data 17, 277–292.
Yi, X., Geng, X., Mo, Y., Zhong, G., Tang, J., Zhu, S., Cheng, Z., Zhao, S., Li, J., Gustafsson, O., Peng, P., Zhang, G., 2023. Compound-specific radiocarbon analysis of benzene polycarboxylic acids for source apportionment of polyaromatic organic matter in ambient aerosols. Atmos. Environ. 307 (8), 119832.
Yi, X., Zhong, G., Geng, X., Tang, J., Lin, B., Zhu, S., Gao, S., Yao, C., Cheng, Z., Zhao, S., Li, J., Zhang, G., 2024. Dual-carbon isotope analysis of benzene polycarboxylic acids for tracking black carbon across different environments. Appl. Geochem. 170 (8), 106062.
Yin, J., Xie, X., Wei, X., Zhang, H., Ying, Q., Hu, J., 2024. Source-specified atmospheric age distribution of black carbon and its impact on optical properties over the Yangtze River Delta. Sci. Total Environ. 923, 171353.
Yu, K., Xing, Z., Huang, X., Deng, J., Andersson, A., Fang, W., Gustafsson, Ö., Zhou, J., Du, K., 2018. Characterizing and sourcing ambient $PM_{2.5}$ over key emission regions in China III: carbon isotope based source apportionment of black carbon. Atmos. Environ. 177, 12–17.
Zaveri, R.A., Barnard, J.C., Easter, R.C., Riemer, N., West, M., 2010. Particle-resolved simulation of aerosol size, composition, mixing state, and the associated optical and cloud condensation nuclei activation properties in an evolving urban plume. J. Geophys. Res. 115, D17210.
Zelenay, V., Monge, M.E., D'Anna, B., George, C., Styler, S.A., Huthwelker, T., Ammann, M., 2011. Increased steady state uptake of ozone on soot due to UV/Vis radiation. J. Geophys. Res. Atmos. 116, D11301.
Zencak, Z., Elmquist, M., Gustafsson, Ö., 2007. Quantification and radiocarbon source apportionment of black carbon in atmospheric aerosols using the CTO-375 method. Atmos. Environ. 41, 7895–7906.
Zeng, L., Tan, T., Zhao, G., Du, Z., Hu, S., Shang, D., Hu, M., 2024. Overestimation of black carbon light absorption due to mixing state heterogeneity. npj Clim. Atmos. Sci. 7, 2.
Zhang, C., Zhang, B., Ling, Z., Xiao, Y., Li, S., Yu, Y., Zou, B., Chen, X., Shen, M., 2022a. Long-term exposure to ambient black carbon is associated with sleep disturbance in college students. Sci. Total Environ. 838, 156066.
Zhang, F., 2023. The Mixing State of Black Carbon Aerosols and the Effect on Optical Properties. Tsinghua University. Ph.D. thesis, School of Environment.
Zhang, F., Chen, Y., Su, P., Cui, M., Han, Y., Matthias, V., Wang, G., 2021a. Variations and characteristics of carbonaceous substances emitted from a heavy fuel oil ship engine under different operating loads. Environ. Pollut. 284, 117388.
Zhang, F., Guo, H., Chen, Y., Matthias, V., Zhang, Y., Yang, X., Chen, J., 2020a. Size-segregated characteristics of organic carbon (OC), elemental carbon (EC) and organic matter in particulate matter (PM) emitted from different types of ships in China. Atmos. Chem. Phys. 20, 1549–1564.
Zhang, J., Li, X., Cheng, W., Li, Y., Shi, T., Jiang, Y., Wang, T., Wang, H., Ren, D., Zhang, R., Zheng, Y., Tang, J., 2022b. Chronic carbon black nanoparticles exposure increases lung cancer risk by affecting the cell cycle via circulatory inflammation. Environ. Pollut. 305, 119293.

Zhang, J., Liu, J., Tao, S., Ban-Weiss, G.A., 2015. Long-range transport of black carbon to the Pacific Ocean and its dependence on aging timescale. Atmos. Chem. Phys. 15, 11521–11535.
Zhang, J., Zhang, R., Zhang, Y., Zhang, S., Liu, M., 2025a. Accuracy analysis and applicability assessment of MERRA-2 and TAP atmospheric black carbon data over China from 2000 to 2020. Res. Environ. Sci. 38, 569–578.
Zhang, P., Chen, T., Ma, Q., Chu, B., Wang, Y., Mu, Y., Yu, Y., He, H., 2022c. Diesel soot photooxidation enhances the heterogeneous formation of $H_2SO_4$. Nat. Commun. 13, 5364.
Zhang, P., Wang, Y., Chen, T., Yu, Y., Ma, Q., Liu, C., Li, H., Chu, B., He, H., 2023a. Insight into the mechanism and kinetics of the heterogeneous reaction between $SO_2$ and $NO_2$ on diesel black carbon under light irradiation. Environ. Sci. Technol. 57 (MAR), 2023.
Zhang, Q., Wang, Y., Xiao, Q., Geng, G., Davis, S.J., Liu, X., Yang, J., Liu, J., Huang, W., He, C., Luo, B., Martin, R.V., Brauer, M., Randerson, J.T., He, K., 2025b. Long-range $PM_{2.5}$ pollution and health impacts from the 2023 Canadian wildfires. Nature 645, 672–678.
Zhang, R., Peng, J., Wang, Y., Hu, M., 2016. Reply to boucher et al.: rate and timescale of black carbon aging regulate direct radiative forcing. Proc. Natl. Acad. Sci. 113, 5094–5095.
Zhang, S., Sarwar, G., Xing, J., Chu, B., Xue, C., Sarav, A., Ding, D., Zheng, H., Mu, Y., Duan, F., Ma, T., He, H., 2021b. Improving the representation of HONO chemistry in CMAQ and examining its impact on haze over China. Atmos. Chem. Phys. 21, 15809–15826.
Zhang, X., Li, J., Mo, Y., Shen, C., Ding, P., Wang, N., Zhu, S., Cheng, Z., He, J., Tian, Y., Gao, S., Zhou, Q., Tian, C., Chen, Y., Zhang, G., 2019. Isolation and radiocarbon analysis of elemental carbon in atmospheric aerosols using hydropyrolysis. Atmos. Environ. 198, 381–386.
Zhang, X., Wang, Y., Zhang, X., Guo, W., Niu, T., Gong, S., Yin, Y., Zhao, P., Jin, J., Yu, M., 2008. Aerosol monitoring at multiple locations in China: contributions of EC and dust to aerosol light absorption. Tellus Ser. B Chem. Phys. Meteorol. 60, 647–656.
Zhang, Y., Cui, S., Li, J., Wang, M., Xu, X., Wang, J., Fang, J., Lang, H., Zheng, B., Zhong, S., Sun, P., Li, H., Wu, Y., Hu, J., Wang, J., Chen, M., Favez, O., Hauglustaine, D., Ciais, P., Daellenbach, K.R., et al., 2026a. Urban black-carbon radiative heating intensified by biogenic-anthropogenic interactions. Nat. Geosci. 19, 439–446.
Zhang, Y., Liu, Z., Chen, Y., Feng, Y., Cui, M., Feng, X., Peng, Y., Cai, J., Chen, T., 2025c. Size-segregated emission characteristics and associated toxicity of polycyclic aromatic compounds from agricultural machinery. J. Hazard. Mater. 497, 139627.
Zhang, Y., Perron, N., Ciobanu, V.G., Zotter, P., Minguillón, M.C., Wacker, L., Prévôt, A. S.H., Baltensperger, U., Szidat, S., 2012. On the isolation of OC and EC and the optimal strategy of radiocarbon-based source apportionment of carbonaceous aerosols. Atmos. Chem. Phys. 12, 10841–10856.
Zhang, Y., Zhang, Q., Cheng, Y., Su, H., Li, H., Li, M., Zhang, X., Ding, A., He, K., 2018. Amplification of light absorption of black carbon associated with air pollution. Atmos. Chem. Phys. 18, 9879–9896.
Zhang, Y., Zhang, Q., Yao, Z., Li, H., 2020b. Particle size and mixing state of freshly emitted black carbon from different combustion sources in China. Environ. Sci. Technol. 54, 7766–7774.
Zhang, Z., Cheng, Y., Liang, L., Liu, J., 2023b. The measurement of atmospheric black carbon: a review. Toxics 11, 975.
Zhang, Z., Wang, J., Riemer, N., Liu, C., Wang, J., Jin, Y., Tian, Z., Chen, G., Wang, B., Huang, X., Ding, A., Wang, S., 2026b. Inversion approach for inferring mixing state and improving optical estimation of coated black carbon using bulk-volume variables and number-size distributions. Environ. Sci. Technol. 60, 3998–4007.
Zhang, Z., Wang, J., Riemer, N., Wang, J., Liu, C., Jin, Y., Tian, Z., Shen, S., Wang, B., Chen, G., Zhao, B., Hu, J., Wang, M., Su, H., Wang, S., Cheng, Y., Ding, A., 2025d. The droplet activation parameterization for black carbon-containing particles in steady state. Geophys. Res. Lett. 52 e2024GL114433.
Zhao, D., Huang, M., Liu, D., Ding, D., Tian, P., Liu, Q., Zhou, W., Sheng, J., Wang, F., Bi, K., 2018. Aircraft measurements of black carbon in the boundary layer over the North China Plain. Atmos. Chem. Phys. 1–25.
Zhao, G., Yu, Y., Tian, P., Li, J., Guo, S., Zhao, C., 2020. Evaluation and correction of the ambient particle spectral light absorption measured using a filter-based aethalometer. Aerosol Air Qual. Res. 20, 1833–1841.
Zhao, W., Zhao, G., Li, Y., Guo, S., Ma, N., Tang, L., Zhang, Z., Zhao, C., 2022. New method to determine black carbon mass size distribution. Atmos. Meas. Tech. 15, 6807–6817.
Zhao, W., Zhao, Y., Zheng, Y., Chen, D., Xin, J., Li, K., Che, H., Li, Z., Ma, M., Hang, Y., 2024a. Long-term variability in black carbon emissions constrained by gap-filled absorption aerosol optical depth and associated premature mortality in China. Atmos. Chem. Phys. 24, 6593–6612.
Zhao, W., Zhao, Y., Zheng, Y., Chen, D., Xin, J., Li, K., Che, H., Li, Z., Ma, M., Hang, Y., 2024b. Long-term variability in black carbon emissions constrained by gap-filled absorption aerosol optical depth and associated premature mortality in China. Atmos. Chem. Phys. 24, 6593–6612.
Zheng, B., Tong, D., Li, M., Liu, F., Hong, C., Geng, G., Li, H., Li, X., Peng, L., Qi, J., Yan, L., Zhang, Y., Zhao, H., Zheng, Y., He, K., Zhang, Q., 2018. Trends in China's anthropogenic emissions since 2010 as the consequence of clean air actions. Atmos. Chem. Phys. 18, 14095–14111.
Zheng, H., Kong, S., Ding, D., Savadkoohi, M., Song, C., Zheng, M., Harrison, R.M., 2025. Black carbon aerosols in China: Spatial-temporal variations and lessons from long-term atmospheric observations. Atmos. Chem. Phys. 25, 16363–16386.
Zheng, H., Kong, S., Zheng, M., Yan, Y., Yao, L., Zheng, S., Yan, Q., Wu, J., Cheng, Y., Chen, N., Bai, Y., Zhao, T., Liu, D., Zhao, D., Qi, S., 2020. A 5.5-year observations of black carbon aerosol at a megacity in central China: levels, sources, and variation trends. Atmos. Environ. 232, 117581.
Zheng, X., Wu, Y., Jiang, J., Zhang, S., Liu, H., Song, S., Li, Z., Fan, X., Fu, L., Hao, J., 2015. Characteristics of on-road diesel vehicles: black carbon emissions in chinese cities based on portable emissions measurement. Environ. Sci. Technol. 49, 13492–13500.
Zheng, Z., Curtis, J.H., Yao, Y., Gasparik, J.T., Anantharaj, V.G., Zhao, L., West, M., Riemer, N., 2021a. Estimating submicron aerosol mixing state at the global scale with machine learning and Earth system modeling. Earth Space Sci. 8 e2020EA001500.
Zheng, Z., West, M., Zhao, L., Ma, P., Liu, X., Riemer, N., 2021b. Quantifying the structural uncertainty of the aerosol mixing state representation in a modal model. Atmos. Chem. Phys. 21, 17727–17741.
Zhi, G., Chen, Y., Feng, Y., Xiong, S., Li, J., Zhang, G., Sheng, G., Fu, J., 2008. Emission characteristics of carbonaceous particles from various residential coal-stoves in China. Environ. Sci. Technol. 42, 3310–3315.
Zhou, Q., Cheng, C., Yang, S., Yuan, M., Meng, J., Gong, H., Zhong, Q., Zhang, Y., Xie, Y., Zhou, Z., Li, M., 2022. Enhanced mixing state of black carbon with nitrate in single particles during haze periods in Zhengzhou, China. J. Environ. Sci. 111, 185–196.
Zhou, Q., Liu, X., Zhang, T., Liu, Y., Yan, C., Liu, B., Shen, X., Tang, X., Sun, Q., Zhu, T., Zheng, M., 2025. Investigating sources of black carbon in Beijing with receptor model and continuous hourly measurements from 2016 to 2019. Atmos. Environ. 360, 121408.
Zhou, Y., Zhuang, B., Wang, T., Gao, P., Li, S., Hu, Y., Li, M., Cao, H., Xie, M., Chen, H., 2024. Characteristics of urban black carbon aerosols in the Yangtze River Delta of China based on long-term observations. Atmos. Environ. 326, 120488.
Zhu, J., Chen, Y., Shang, J., Zhu, T., 2019. Effects of air/fuel ratio and ozone aging on physicochemical properties and oxidative potential of soot particles. Chemosphere 220, 883–891.
Zhu, J., Shang, J., Chen, Y., Kuang, Y., Zhu, T., 2020. Reactive oxygen species-related inside-to-outside oxidation of soot particles triggered by visible-light irradiation: physicochemical property changes and oxidative potential enhancement. Environ. Sci. Technol. 54, 8558–8567.
Zhu, J., Sheng, M., Shang, J., Kuang, Y., Shi, X., Qiu, X., 2022. Photocatalytic role of atmospheric soot particles under visible-light irradiation: reactive oxygen species generation, self-oxidation process, and induced higher oxidative potential and cytotoxicity. Environ. Sci. Technol. 56, 7668–7678.
Zhu, X., Liu, B., Guo, C., Li, Z., Cheng, M., Zhu, X., Wei, Y., 2023. Short and long-term association of exposure to ambient black carbon with all-cause and cause-specific mortality: a systematic review and meta-analysis. Environ. Pollut. 324, 121086.
Zimmermann, R., 2015. Aerosols and health: a challenge for chemical and biological analysis. Anal. Bioanal. Chem. 407, 5863–5867.
Zuo, B., Wang, F., Li, Z., Yu, B., Zhang, J., Xu, W., Ai, S., Chu, H., 2025. Heat shock protein 70 mitigates black carbon particles-induced cardiac damage. J. Environ. Sci. 156, 871–881.